Topology optimization of Double-Double (DD) composite laminates considering stress control

Yan Wang[1,2], Dan Wang[3,**], Yucheng Zhong [1,2,*], David W. Rosen[3], Shuxin Li[4], Stephen W. Tsai[5]

Abstract

Double-double (DD) laminates are a new type of composite layups, which can achieve different structural properties by adjusting two sets of balanced fiber orientations. The combination of topology optimization and DD laminates can further enhance the advantages of composite materials as lightweight designs. Currently, most topology optimizations use compliance as the target. Existing optimization studies implementing stress control are mostly for isotropic materials. It is a great challenge to implement stress control during topology optimization of composite laminates, because the layer-wisely distributed stress brings a lot of design constraints and leads to many local optima. In this paper, we propose a nested p-norm method that integrates failure indexes of different elements in different layers into one design response, thus realizing the effective stress control for topology optimization of laminated structures. There are two levels of p-norm nested in the process: the inner p-norm approximates the maximum failure index of all the layers for one element, and the outer p-norm approximates the maximum failure index for all elements. The nested p-norm scheme is implemented under the framework of the Solid Isotropic Material with Penalization (SIMP) model, which is extended to DD laminates by interpolating the stiffness matrix of composites. Then, the optimization model is established by minimizing the maximum Tsai-Hill failure index using the function formulated by the proposed nested p-norm method under the constraint of the structural volume fraction and compliance. Next, stress sensitivities are calculated using the adjoint method. It is noticeable that the sensitivity with respect to the filtered projection density is separately calculated to improve the computational efficiency. Finally, typical examples of topology optimization with stress singularity such as an L-shaped bracket, a crack problem, a corbel structure, and an antenna support bracket are given. It is validated that the proposed nested p-norm method can effectively and efficiently reduce the stress concentration of laminate structures compared with the methods using single p-norm and layer-wise p-norm. Additionally, the optimization results show that the DD laminate has similar optimized configurations and optimization effects as those of the conventional Quad laminate with the equivalent stiffness.

Keywords: double-double (DD) laminates; composites; topology optimization; stress; Tsai-Hill failure criterion

1. Introduction

Topology optimization is one of the most active research topics in the field of structural optimization for academic research because it can optimally distribute materials and effectively reduce the weight of structures. Most of the early topology optimization research focused on maximizing stiffness, that is, minimizing compliance [1-3] using the popular Solid Isotropic Material with Penalization (SIMP) method proposed by Bendsoe [4,5] by interpolating the elemental pseudo densities exponentially. The evolutionary structure optimization (ESO) method is an alternative way to update the structural topology by gradually removing ineffective or inefficient materials and/or adding

[1] Hubei Key Laboratory of Theory and Application of Advanced Materials Mechanics, School of Science, Wuhan University of Technology, Wuhan 430070, P. R. China
[2] School of Science, Wuhan University of Technology, Wuhan 430070, P. R. China
[3] Institute of High Performance Computing (IHPC), Agency for Science, Technology and Research (A*STAR), 1 Fusionopolis Way, #16-16 Connexis, 138632, Republic of Singapore
[4] State Key Laboratory of Materials Synthesis and Processing, Wuhan University of Technology, Wuhan 430070, P.R. China
[5] Department of Aeronautics and Astronautics, Stanford University, Stanford, CA 94305, USA
* Corresponding author. Email: YZHONG1@e.ntu.edu.sg
** Co-corresponding author. Email: wangd@ihpc.a-star.edu.sg

effective materials [6-9]. Then, a level-set method defined the structural topology change using a shape variation in a higher order surface [10-13], which bridges shape optimization and topology optimization by providing smooth shape boundaries with an implicit topologic description. Recently, new technologies, such as multiscale analysis [14-15], reduced order modeling [16-17], isogeometric analysis (IGA) [18-19], the phase field method [20], geometric feature driving method [21-23], and topological derivative method [24-25] were also used to solve topology optimization problems. At the same time, density filtering [26] and projection strategies [27-29], were also investigated to avoid the checkerboard phenomenon and achieve clear optimal topology, respectively.

Adding stress control to topology optimization has always been a difficult yet important research problem [30-32]. Numerical examples of a typical L-shaped bracket structure showed a big stress concentration at the corner using the optimal configuration from topology optimization for compliance minimization [33]. There are three important challenges in dealing with topology optimization including stress control: i) stress is a local response and correlated to the existence of the associated element, which leads to a fake stress for elements with a very small density (for approximating no material state); ii) as local responses, the stresses of all the elements in the design domain have to be constrained to realize the stress control, which will introduce a large number of design constraints and bring an unbearable burden to the optimization process; iii) stresses are highly nonlinear with respect to the structural topology and form a non-convex optimization problem.

Cheng and Guo [34] proposed an ε relaxation method and Bruggi [35] proposed a *qp* relaxation model to alleviate the stress problem mentioned in the first challenge. To solve the second challenge, many techniques have been proposed to integrate the stresses of different elements into one expression to make the optimization affordable. It includes p-norm [36-37], KS function [38-39], and a fusion or a variation of two or more of the above technologies [8, 40-41]. Besides, an augmented Lagrange method [42-43] was proposed to reformulate the stress constraints to new Lagrange function. A clustering technique was proposed to cluster the stress evaluation points into groups using a modified p-norm for computation efficiency improvement [37]. A machine-learning-assisted parameterization has been used to implement an algebraic stress model [44]. Optimization algorithms of the method of moving asymptotes (MMA) and its extensions [45-47] are available to solve the last challenge of the nonlinear nature of stress in the optimization process. By combining the above techniques to deal with the stress problems, the methods used for compliance minimization in topology optimization were successfully extended to stress-constrained topology optimization. A combination of a B-spline finite cell method and level set function solved the concurrent shape and topology optimization considering stress constraints in a fixed Eulerian mesh [48] and this method was extended to free-form design domains [49-51]. More work of topology optimization considering stress constraints has been done on thermoelastic structures [52-53], piezoresistive sensors [54], while considering uncertainty and variability in loading, geometry and material properties [55]. However, current studies for topology optimizations considering stress constraints were mostly for isotropic materials assuming the same tensile and compressive strengths. For isotropic materials with different tensile and compressive strengths, the topology optimization results considering stress constraints showed that the improved optimization model can take advantage of the heterogeneous strengths of materials to further improve the load-carrying capacity of the structure [56].

Laminated composites offer a possibility to achieve high specific strength, specific stiffness, and specific stability by manipulating their stacking sequence. Thus, they are widely used in aerospace and ground transportation industries. It is proved that topology optimization could help reduce the structural compliance of two-material composites [57], composite laminates [58], composite sandwich structures [59] by rearranging the load-bearing path. It should be noted that when designing composite structures, not only structural stiffness but also structural strength is an important indicator, especially for load-bearing structures that are prone to stress singularities [60]. Optimization of composites with variable stiffness laminates [61-64] and non-uniformly distributed curved stiffeners [65-68] have brought about significant enhancement in the structural strength and buckling load by optimally tailoring the material distribution of composites.

However, considering stress control during topology optimization of composite materials is an even more difficult task. On one hand, composite materials are composed of constituents of distinct mechanical properties, thus exhibiting anisotropic material properties. The failure strengths of a composite structure are different along different directions [69,70]. The constitutive equation of the material is much more complex. On the other hand, composite laminates are composed of multiple layers, which bear different loads and consequently present different failure modes, leading to significantly increased stress constraints. Because of these technical difficulties, there are few studies on topology optimization of composite structures considering stress control.

Double-double (DD) laminates are an innovative composite layup proposed by Tsai [71]. DD laminates consist of two sets of balanced plies. It is a strong replacement to the conventional Quad layup consisting of fibers orientated exclusively along 0°, 90° and 45°. Therefore, DD laminates can offer much larger design space. It is shown that DD laminates have the advantages of better tailoring, cheaper manufacturing cost, and easy tapering, and thus open huge potential optimization opportunities for stiffness, strength, and buckling improvement [71-74]. Thus, DD laminates will be a promising replacement of the conventional Quad laminates.

In this paper, we focus on topology optimization of DD composite laminates considering stress control. A nested p-norm method based on a composite failure criterion is proposed and the optimization problem is formulated aiming to solve the above-mentioned challenges. Details of the proposed method are presented in Section 2. Then, the involved sensitivity calculations are provided in Section 3. After that, typical examples with high stress concentrations including an L-shaped bracket, a crack problem, a corbel structure, and an antenna support bracket are presented in Section 4 to demonstrate the effectiveness of the proposed method. Finally, conclusions are given in Section 5.

2. Topology optimization of DD laminates considering stress control

Topology optimization is an optimization technique to improve the structural properties by optimizing the material distribution. As illustrated in Figure 1, the structural topology will be changed by creating holes inside the design domain via deleting materials.

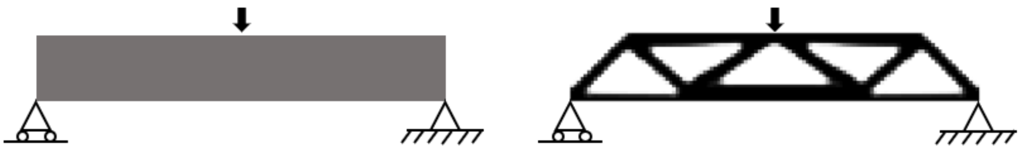

(a) Initial design domain (b) Optimal topology for a maximum stiffness

Figure 1. Schematic illustration of the topology optimization process.

This section will introduce the key technologies in topology optimization of the novel double-double (DD) laminates considering stress control. Firstly, the material stiffness matrix is defined for DD laminate. Secondly, the SIMP material interpolation model is extended to DD laminates. Thirdly, the stress singularity and its interpolation model are introduced. Fourthly, the Tsai-Hill failure criterion is given, and its nested p-norm formulation is proposed to reduce the number of stress constraints for an affordable optimization procedure. Finally, mathematical optimization models are established, and the optimization process is given for topology optimization of DD laminates considering stress control.

2.1 Material stiffness matrix of DD laminates

The constitutive equation of a composite laminate is calculated as an integral resultant along the laminate thickness with the following expression:

$$\begin{bmatrix} \mathbf{N} \\ \mathbf{M} \end{bmatrix} = \begin{bmatrix} \mathbf{A} & \mathbf{B} \\ \mathbf{B} & \mathbf{D} \end{bmatrix} \begin{bmatrix} \boldsymbol{\varepsilon}_0 \\ \boldsymbol{\kappa} \end{bmatrix} \tag{1}$$

where **N** and **M** are the force and moment resultants, respectively. **A**, **D**, and **B** matrices are the extensional, bending, and coupling material stiffness matrices, respectively. $\boldsymbol{\varepsilon}_0$ and $\boldsymbol{\kappa}$ are the mid-plane strains and curvatures, respectively. The **A**, **B**, and **D** matrices are calculated as an integral resultant along the laminate thickness with the expression of:

$$A_{ij} = \sum_{k=1}^{n} \bar{Q}_{ij}(z_k - z_{k-1}),\ B_{ij} = \sum_{k=1}^{n} \frac{\bar{Q}_{ij}}{2}(z_k^2 - z_{k-1}^2),\ D_{ij} = \sum_{k=1}^{n} \frac{\bar{Q}_{ij}}{3}(z_k^3 - z_{k-1}^3) \qquad (2)$$

where, $\bar{Q}_{ij}$ is the component at the *i*th row and *j*th column of the material stiffness matrix. The derivation of the $\bar{Q}_{ij}$ matrix follows classical lamination theory.

A single layer of a laminate can be seen as an orthotropic material. For plane-stress scenario, the stress-strain relationship of a single layer is given by:

$$\begin{bmatrix} \sigma_1 \\ \sigma_2 \\ \tau_{12} \end{bmatrix} = \begin{bmatrix} Q_{11} & Q_{12} & 0 \\ Q_{12} & Q_{22} & 0 \\ 0 & 0 & Q_{66} \end{bmatrix} \begin{bmatrix} \varepsilon_1 \\ \varepsilon_2 \\ \gamma_{12} \end{bmatrix} \qquad (3)$$

where '1' denotes the fiber direction, and '2' denotes the direction perpendicular to the fiber in the same plane. The terms of the stiffness matrix **Q** are given by:

$$Q_{11} = \frac{E_1}{1-\nu_{12}\upsilon_{21}},\quad Q_{22} = \frac{E_2}{1-\upsilon_{21}\upsilon_{12}},\quad Q_{12} = \frac{\upsilon_{12}E_2}{1-\upsilon_{12}\upsilon_{21}},\quad Q_{66} = G_{12} \qquad (4)$$

For an arbitrary ply with a fiber orientation of θ with respect to the global Cartesian coordinate system, as shown in Figure 2, the terms of the stiffness matrix $\bar{\mathbf{Q}}$ are given in the global system by:

$$\bar{\mathbf{Q}} = \mathbf{TQT}^T \qquad (5)$$

$$\boldsymbol{T} = \begin{bmatrix} \cos^2\theta & \sin^2\theta & -2\cos\theta\sin\theta \\ \sin^2\theta & \cos^2\theta & 2\cos\theta\sin\theta \\ \cos\theta\sin\theta & -\cos\theta\sin\theta & \cos^2\theta - \sin^2\theta \end{bmatrix} \qquad (6)$$

where **T** is the rotation matrix corresponding to the angle θ.

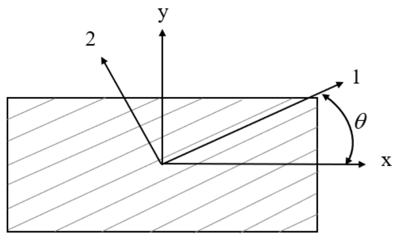

Figure 2. Rotation from the local 1-2 to the global *x*-*y* coordinate system.

DD laminates are novel layups including two group of balanced angles in the form $[\pm\Phi/\pm\Psi]_r$, where *r* represents the number of repeats. The

Current composite structural design is dominated by using Quad layups as a combination of different plies of 0, ±45, and 90 degrees, as illustrated in Figure 3(a), where the symmetric layup is required to achieve zero extension-bending coupling. Quad laminates were originally used because of the inability to precisely lay plies at any angle. With the development of automatic cutting device and automatic positioning device, it has been easy to realize the layup of any angle. Double-double (DD) laminates are novel layups proposed by Tsai [71] made up of two pairs of balanced ply orientations, and the four angles work as thin-assembly building blocks to be repeated to form the whole laminate layup, as illustrated in Figure 3(b). By choosing the layup sequence of [Φ/-Ψ/-Φ/Ψ] for one representative sub-laminate, DD does not require a symmetric layup to achieve homogenization with an insignificant coupling matrix **B** after 3 or 4 repeats, while at the same time, the normalized **A** and **D** matrices are equal, which can further simplify the laminate design by eliminating the effect of laminate sequences.

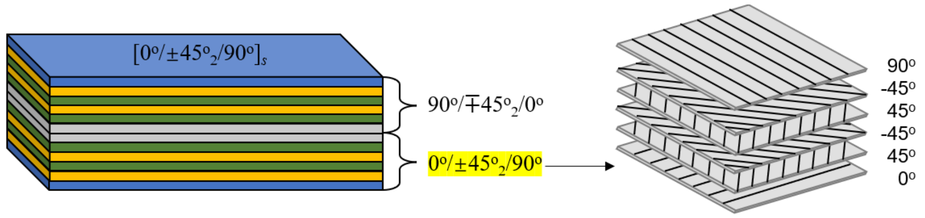

(a) A Quad layup

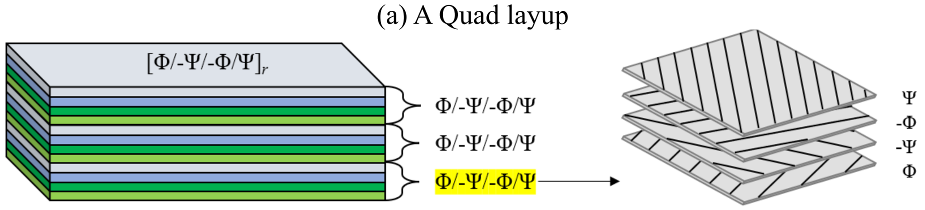

(b) A DD layup

Figure 3. Illustration of the layups of traditional Quad and DD laminates.

The limited angles of laminate layups, as well as the requirement of symmetrical layups, greatly restricts the design space of Quad layups. At the same time, there are thousands of stacking sequence permutations of Quad layups without uniqueness criteria, which greatly increases the number of invalid duplicate solutions in the design, largely wasting the search time. Unlike the discrete nature of Quad, DD laminates are field-based and can offer a laminate with any values of fiber orientations. The flexibility of DD makes it can match all Quad laminates with extraordinarily simple stack-up under the equivalent stiffness. For instance, it was recently reported that an airplane wing skin with hundreds of local laminates can be replaced by one DD [71], which is an example of the DD revolution that is motivating many company engineers.

2.2 SIMP material interpolation model for laminates

The Solid Isotropic Material with Penalization (SIMP) method is a commonly used material interpolation method proposed by Bendsoe [5]. The core of the SIMP method is to push local material pseudo densities to approach either one or zero to achieve a black and white only material distribution, as illustrated in Figure 1(b). The main procedure of using a SIMP model is given below. Firstly, the design domain is discretized into a finite element mesh, where each element is assigned a pseudo density between 0 and 1 as a design variable with 0 representing void material and 1 representing solid material. Then, a penalty mechanism of a power-law relationship between material properties and elemental pseudo densities is introduced for intermediate densities, which are expected to be eliminated as much as possible in the optimal material distribution. The formulation of the penalty function is expressed as:

$$\mathbf{C}_e(x_e) = x_e^k \mathbf{C}_0 \tag{7}$$

where $\mathbf{C}_0$ and $\mathbf{C}_e$ represent the ABD matrix of the solid material, as calculated in Eq. (2), and that of the e^{th} element, respectively; x_e is the pseudo density of the e^{th} element, and k is the penalty factor. The influence of k is illustrated in Figure 4. It is usually set to 3 or 4 since it cannot be too small to ensure the effective penalty effect, nor too large to avoid numerical singularities. In addition, the density filtering strategy and the projection method adopted in the current study are provided in the Appendix.

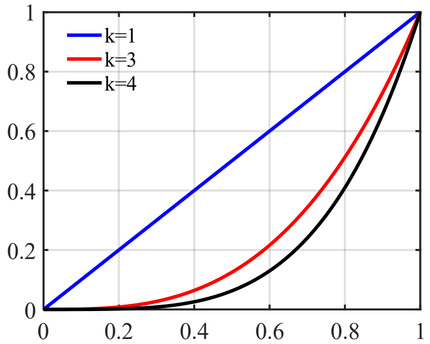

Figure 4. Influence of the penalty factor in SIMP model.

2.3 The stress singularity and its interpolation model

Stress is a local property associated to the specific area of an element or a node in a simulation using the finite element method (FEM). The value of stress not only depends on the pseudo density of the associated element, but also is related to the existence of the element. When the element is fully eliminated, the stress should directly drop to zero since the attached material is removed. However, in the FEM implementation, the void state of material is realized using a very small density. The non-zero density of elements causes small stresses to remain, that leads to many local minima having intermediate pseudo densities. To avoid the stress singularity and effectively approach a clear topology, there are two common ways to interpolate the stress: (1) ε relaxation [34], and (2) *qp* relaxation [35]. In general, *qp* relaxation is considered as a more convenient and superior alternative to ε relaxation. Thus, *qp* relaxation is used in this paper to reduce the stress of elements with a low density.

In *qp* relaxation [35], stresses of elements with intermediate densities are penalized based on those of the solid material with the expression of:

$$\boldsymbol{\sigma}_e^* = \rho_e^s \hat{\boldsymbol{\sigma}}_e^* \tag{8}$$

where $\boldsymbol{\sigma}_e^*$ is the penalized stress, s is the penalization factor with the commonly used value of 0.5 [55] on the elemental projection density of ρ_e defined in Eq. (A3), and $\hat{\boldsymbol{\sigma}}_e^*$ is the elemental stresses of the solid material before penalization, with the superscript * representing the quantities at the local material coordinate system (1-2 coordinate system). The expression of $\hat{\boldsymbol{\sigma}}_e^*$ is given as:

$$\hat{\boldsymbol{\sigma}}_e^* = \mathbf{Q}_0^T \mathbf{T}^T \mathbf{B}_e \mathbf{u}_e \tag{9}$$

where $\mathbf{u}_e$ is the nodal displacement vector related to the e^{th} element, $\mathbf{B}_e$ is the strain-displacement tensor, and $\mathbf{Q}_0$ is the material stiffness of solid material as expressed in Eq. (4). It is noticeable that in Eq. (9), the displacement vector $\mathbf{u}_e$ is evaluated at the global coordinate system, while $\boldsymbol{\sigma}_e^*$ and $\hat{\boldsymbol{\sigma}}_e^*$ are evaluated at the local 1-2 coordinate system with direction '1' representing the fiber direction and direction '2' representing the transverse direction, since the Tsai-Hill failure criterion is evaluated in the local coordinate system.

The above formulation ensures that the penalized stress is identical to the real stress when the elemental pseudo density approaches to 0 or 1. It is noticeable that the elemental stress penalty with intermediate densities increases disproportionately to avoid the occurrence of excessive intermediate densities and reduce the stress singularity at low densities.

2.4 Tsai-Hill failure criterion and its nested p-norm for composite laminates

The anisotropic nature of composite materials requires independent strength evaluations along different directions instead of one Von-Mises stress. The Tsai-Hill failure criterion [69,70] is commonly used to assess the failure state of a composite laminate by integrating different stress components and strength values together, which is expressed as:

$$F_{\mathrm{TH}} = \frac{\sigma_1^2}{X^2} + \frac{\sigma_2^2}{Y^2} - \frac{\sigma_1\sigma_2}{X^2} + \frac{\tau_{12}^2}{S^2} \tag{10}$$

where σ_1, σ_2, and τ_{12} are the tensile/compressive stresses along 1 and 2 directions in the local coordinate system, and in-plane shear, respectively; X, Y, and S are their corresponding ultimate strength values. The Tsai-Hill failure index denoted by F_{TH} will degrade to the Von Mises failure criterion for isotropic materials when $X=Y=\sqrt{3}S$, where $F_{\mathrm{TH}}=1$ is a transition state with the value larger than 1 representing material failure. The above equation can also be rewritten in a matrix form as:

$$F_{\mathrm{TH}} = \boldsymbol{\sigma}^{*T}\mathbf{M}_{\mathrm{TH}}\boldsymbol{\sigma}^{*} \tag{11}$$

where $\boldsymbol{\sigma}^*$ is the stress vector in the local 1-2 coordinate system and $\mathbf{M}_{\mathrm{TH}}$ is the failure strength tensor with the expressions of:

$$\boldsymbol{\sigma}^{*} = [\sigma_1 \ \sigma_2 \ \tau_{12}]^T \tag{12}$$

$$\mathbf{M}_{\mathrm{TH}} = \begin{bmatrix} \frac{1}{X^2} & \frac{-1}{2X^2} & 0 \\ \frac{-1}{2X^2} & \frac{1}{Y^2} & 0 \\ 0 & 0 & \frac{1}{S^2} \end{bmatrix} \tag{13}$$

Similar to the case of isotropic materials, the number of stress constraints in composites, which is expressed in Tsai-Hill failure indexes, also needs be reduced in order to make the sensitivity calculation affordable. However, there are multiple layers for each element, whose responses have to be evaluated individually. Therefore, the number of strength evaluations for composites is obviously more than isotropic materials. It is possible to combine all the Tsai-Hill failure indexes into one p-norm function, as used in isotropic materials, with the expression of:

$$F_{p_1} = \left(\sum_{i=1}^{n_{\mathrm{L}}} \sum_{e=1}^{n_{\mathrm{E}}} \left(F_{\mathrm{TH}}^{\{i,e\}} \right)^p \right)^{\frac{1}{p}} \tag{14}$$

where $F_{\mathrm{TH}}^{\{i,e\}}$ denotes the Tsai-Hill failure index of the e^{th} element at the i^{th} layer and its expression is available in Eqs. (10) and (11), with the superscript $\{i,e\}$ used to identify the ply sequential number i and the element sequential number e, respectively with $i=1,2, \ldots, n_{\mathrm{L}}$ and $e=1,2,\ldots,n_{\mathrm{E}}$ and n_{L} and n_{E} representing the total numbers of all the plies and all the elements, respectively. p is the exponent of the p-norm function. However, the implementation of the one p-norm method using Eq. (14) shows a lot of numerical instability. The reason for this phenomenon is that the large number of local constraints leads to many local optimal solutions, making it difficult to reach a reasonable optimal solution.

Alternatively, the failure indexes can be integrated together in a layer-wise manner with the expression of:

$$F_{p_2}^{\{i\}} = \left(\sum_{e=1}^{n_{\mathrm{E}}} \left(F_{\mathrm{TH}}^{\{i,e\}} \right)^p \right)^{\frac{1}{p}} \tag{15}$$

The above equation for layer-wise p-norm uses an increased number of stress constraints, which will remarkably increase the computational burden.

In this paper, a nested p-norm approach is proposed to overcome the above problems in the one p-norm method using Eq. (14) and the layer-wised p-norm method using Eq. (15). The nested p-norm formulation is constructed as follows:

$$F_{\mathrm{N}} = \left(\sum_{e=1}^{n_{\mathrm{E}}} (F_e)^p \right)^{\frac{1}{p}} \tag{16}$$

where,

$$F_e = \left(\sum_{i=1}^{n_{\mathrm{L}}} \left(F_{\mathrm{TH}}^{\{i,e\}} \right)^q \right)^{\frac{1}{q}} \tag{17}$$

with F_e and F_{N} representing the inner and outer p-norms for the e^{th} element and for the whole design domain, respectively. Thus, there are two levels of p-norms nested in this process. The inner p-norm approximates the maximum Tsai-Hill failure index of all the layers for one element, and the outer p-norm approximates the maximum value for all elements. By using the nested p-norm approach, only one approximation of the maximum representative of all layers for one element participates in the p-norm combination between elements. This procedure can downgrade the calculation of composite laminates to the p-norm method used in isotropic materials, which effectively reduces the calculation scale and ensures the stability of the calculation to a certain extent. In Eqs. (16) and (17), the outer and inner p-norms have independent exponents p and q. When p and q keep increasing to infinity, the prediction by Eq. (17) is approaching to the maximum Tsai-Hill failure index. However, similar to the p-norm method used for isotropic materials, a big p or q will lead to numerical instability. Therefore, a proper value of p and q needs to be selected. It is recommended to use p=8, and q=10, as adopted in the numerical examples of the current paper. q can be set bigger than p, since the nonlinear influence of the inner layer on the problem is not as great as that of the outer layer.

There are three underlying reasons for using the nested p-norm for strength evaluation of the DD laminate by packing the elemental strength indexes together as the inner p-norm. Firstly, in DD laminates, all the ply angles appear in pairs. For the same element, the plies with paired angles share the same in-plane strain and have the same contribution to the through-thickness stiffness except the coupling items. So, the strength index distributions are very similar for the plies with paired angles, which will increase the number of local minima in the optimization process. If we packed the elemental strength indexes together, the evaluation would be performed among different elements, which would highly reduce the nonlinearity of the problem and the risk of getting trapped in local optima. Secondly, if the angles are also included as design variables in the future, the same DD angles with different stacking sequences will add more local optimal. In other words, the same angles but different stacking sequences will lead to the same strength distribution for in-plane loading. Evaluating the strength at the element level can reduce this complexity. Lastly, the elemental strength can be analogous to the stress distribution for isotropic material for better illustration of the strength distribution of composite laminates at the elemental level.

Compared with other two methods expressed in Eqs. (14) and (15), the nested p-norm method can overcome the problem of a largely increased number of local optima in using one p-norm, and at the same time, effectively increase the computational efficiency compared with the layer-wise p-norm by reducing the strength constraints from the number of composite layups to just one. Moreover, it should be noticed that the proposed nested p-norm can be combined with different failure criteria, not only the Tsai-Hill failure criterion used in this paper.

2.5 Optimization model and implementation procedure

It should be noticed that the proposed nested p-norm method works for different optimization models, such as minimizing the structural weight under the constraints of both stress and compliance. Here, the optimization model is set to minimize the maximum Tsai-Hill failure index with the same structural volume fraction constraints to make the optimal results more comparable among different laminate designs using the conventional Quad and the proposed DD layups with the equivalent stiffness, and also the ones using different DD angles. The weight and volume constraints are interchangeable if the entire structure is composed of the same material. Moreover, an additional compliance constraint with a high upper limit is used to improve the convergence of the optimization process. Thus, the mathematical optimization model is formulated as:

$$\begin{cases} \text{Find: } \mathbf{x} = \{x_1, x_2, \dots, x_e, \dots x_{n_\mathrm{E}}\} \\ \text{Min: } F_\mathrm{N} = \left(\sum_{e=1}^{n_\mathrm{E}} \left(F_e(\mathbf{x})\right)^p \right)^{1/p} \\ s.t. \begin{cases} v_\mathrm{F}(\mathbf{x}) = \dfrac{1}{V} \sum_{e=1}^{n_\mathrm{E}} (\rho_e(\mathbf{x}) V_e) \le v_{\mathrm{F}_0} \\ C(\mathbf{x}) = \dfrac{1}{2} \mathbf{U}^T \mathbf{K} \mathbf{U} \le C_0 \\ \underline{\mathbf{x}} \le \mathbf{x} \le \overline{\mathbf{x}} \end{cases} \end{cases} \tag{18}$$

where $\mathbf{x}$ is the vector of design variables having the physical meaning of pseudo densities of each element with $\underline{\mathbf{x}}$ and $\overline{\mathbf{x}}$ representing its lower and upper bounds, respectively. The pseudo densities are constrained within (0,1]. F_N is the objective with the physical meaning of the nested p-norm of the Tsai-Hill failure indexes of all the elements at all the layers, and F_e is the elemental p-norm for all the layers for the e^{th} element expressed in Eq. (17). n_E is the total number of elements in the design domain. v_F and v_{F_0} are the volume fractions of the current and target materials, respectively. ρ_e is the elemental pseudo density after filtering and projection. V and V_e are the total and the elemental volumes, respectively. C is the structural compliance with C_0 as its upper limit. Here, a large C_0 value is used to guide the convergence of the optimization and the compliance constraint is inactive at the final solution.

As a comparison, the optimization model to minimize the compliance without any stress control is also provided below.

$$\begin{cases} \text{Find: } \mathbf{x} = \{x_1, x_2, \dots, x_e, \dots x_{n_\mathrm{E}}\} \\ \text{Min: } C(\mathbf{x}) = \dfrac{1}{2} \mathbf{U}^T \mathbf{K} \mathbf{U} \\ s.t. \begin{cases} v_\mathrm{F}(\mathbf{x}) = \dfrac{1}{V} \sum_{e=1}^{n_\mathrm{E}} (\rho_e(\mathbf{x}) V_e) \le v_{\mathrm{F}_0} \\ \underline{\mathbf{x}} \le \mathbf{x} \le \overline{\mathbf{x}} \end{cases} \end{cases} \tag{19}$$

There are three main aspects in the implementation of the proposed nested p-norm method for topology optimization of DD laminates with stress control: 1) simulation; 2) design response calculation and their sensitivity analysis; 3) optimization for design variable updating. The optimization procedure is provided in Figure 5, including many implementation details including the density filtering and projections, performance extraction, sensitivity correction, and the convergence judgment. The method of moving asymptotes (MMA) [45] is adopted here as the optimization solver.

During the implementation of MMA, a relatively small step size is used at the beginning of the optimization process in order to maintain the computational stability and avoid falling into local optima. The step size will be gradually increased after several iterations to accelerate the optimization process. Similarly, a small β value for density projection, as defined in Eq. (A3) in Appendix, is used at the beginning, and gradually increased in the optimization process to prevent the solution from falling into a local optimum at the early stage, and at the same time avoid numerical singularity problems. Moreover, the involved sensitivity equations are derived in detail in the next section.

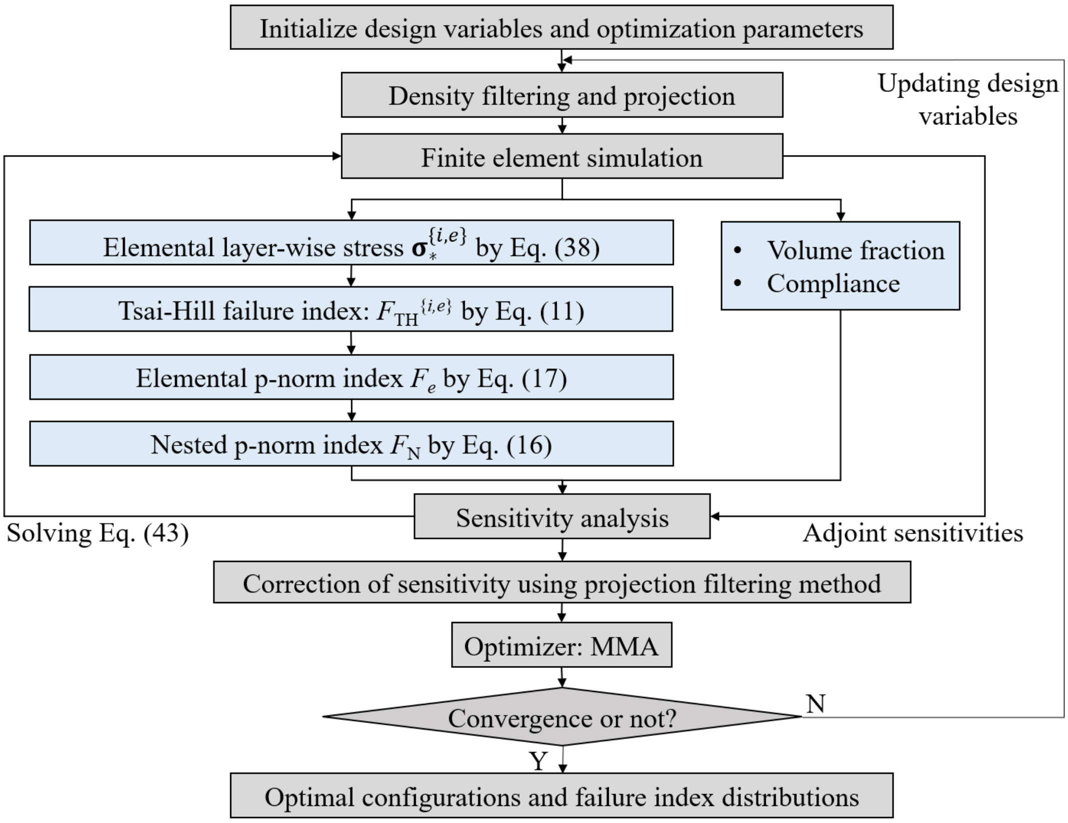

Figure 5. Schematic diagram of the optimization procedure.

3. Sensitivity analysis

In the simulation, all the structural responses are calculated based on the pseudo density after filtering and projection, as provided in the appendix. Hence, the sensitivities with respect to design variables are calculated using the chain rule:

$$\frac{\partial f}{\partial x_e} = \sum_{j=1}^{n_{\mathrm{E}}} \sum_{k=1}^{m} \left(\frac{\partial f}{\partial \rho_j} \frac{\partial \rho_j}{\partial \tilde{x}_{e_k}} \frac{\partial \tilde{x}_{e_k}}{\partial x_e} \right) \tag{20}$$

where f is a general design response, x_e is the pseudo density of the e^{th} element, $\tilde{x}_{e_k}$ is the filtered pseudo density of the e_h element expressed in Eq. (A1), with e_k representing the k^{th} element number in the filtered radius of the e^{th} element, and ρ_j is the j^{th} projection density after projection filtering. m is the total number of elements in the filtering area and n_{E} is the total number of elements.

The above formulation can be rewritten as follows to improve the calculation efficiency:

$$\frac{\partial f}{\partial x_e} = \sum_{j=1}^{n_{\mathrm{E}}} \left\{ \frac{\partial f}{\partial \rho_j} \left[\sum_{k=1}^{m} \left(\frac{\partial \rho_j}{\partial \tilde{x}_{e_k}} \frac{\partial \tilde{x}_{e_k}}{\partial x_e} \right) \right] \right\} \tag{21}$$

where, the last two terms are derived from Eq. (A3) as follows:

$$\frac{\partial \tilde{x}_{e_k}}{\partial x_e} = w_e \tag{22}$$

$$\frac{\partial \rho_j}{\partial \tilde{x}_{e_h}} = \frac{\beta\,(1-\tanh^2(\beta(\tilde{x}_{e_h}-\eta)))}{\tanh(\beta\eta)+\tanh(\beta(1-\eta))} \tag{23}$$

In the implementation of Eq. (20), each derivative of pseudo-density needs to go through at least three layers of derivatives. At the same time, there are also many layers of summation. This not only adds a lot of difficulties in the formulation, but also greatly increases the computation burden. In the expression of Eq. (21), the sensitivity with respect to the projection density is separated from the filtering and projection sensitivities to reduce the number of calculations. This operation will highly enhance the computational efficiency to achieve the same sensitivities. Numerical examples show that computations are sped up by at least 30%.

Based on Eq. (21), sensitivities of volume, compliance, Tsai-Hill failure indexes and their nested p-norm are derived below only with respect to the projection densities for brevity.

3.1 Sensitivities of the compliance and the volume fraction

The sensitivity of the compliance is expressed as:

$$\frac{\partial C}{\partial \rho_j} = \frac{1}{2}\left(\frac{\partial \mathbf{u}^T}{\partial \rho_j}\mathbf{K}\mathbf{u} + \mathbf{u}^T\frac{\partial \mathbf{K}}{\partial \rho_j}\mathbf{u} + \mathbf{u}^T\mathbf{K}\frac{\partial \mathbf{u}}{\partial \rho_j}\right) \tag{24}$$

The equilibrium equation for FEM simulation is expressed as:

$$\mathbf{K}\mathbf{u} = \mathbf{F} \tag{25}$$

where **K** is the stiffness matrix, **u** is the displacement vector and **F** is the force displacement. The stiffness matrix is an assembly of the elemental stiffness with the expression of:

$$\mathbf{K} = \sum_{e=1}^{n_{\mathrm{E}}} \mathbf{K}_e \tag{26}$$

$$\mathbf{K}_e = \int \mathbf{B}_e^T\mathbf{C}_e\mathbf{B}_e d\Omega_e = \rho_e^k \int \mathbf{B}_e^T\mathbf{C}_o\mathbf{B}_e d\Omega_e \tag{27}$$

One pseudo density only affects the local stiffness matrix of the same element. So, the sensitivity of the stiffness matrix is expressed as:

$$\frac{\partial \mathbf{K}}{\partial \rho_j} = \frac{\partial \mathbf{K}_j}{\partial \rho_j} = \frac{k}{\rho_j}\mathbf{K}_j \tag{28}$$

By taking derivative of Eq. (25), it is obtained that:

$$\frac{\partial \mathbf{K}}{\partial \rho_j}\mathbf{u} + \mathbf{K}\frac{\partial \mathbf{u}}{\partial \rho_j} = \mathbf{0} \tag{29}$$

By substituting Eq. (28) into Eq. (29), the sensitivity with respect to the displacement vector, as one unknown in Eq. (24), is expressed as:

$$\frac{\partial \mathbf{u}}{\partial \rho_j} = -\mathbf{K}^{-1}\frac{\partial \mathbf{K}}{\partial \rho_j}\mathbf{u} = -\frac{k}{\rho_j}\mathbf{K}^{-1}\mathbf{K}_j\mathbf{u} \tag{30}$$

By left multiplying Eq. (30) with $\mathbf{u}^T\mathbf{K}$, it is obtained that:

$$\mathbf{u}^T\mathbf{K}\frac{\partial \mathbf{u}}{\partial \rho_j} = -\frac{k}{\rho_j}\mathbf{u}^T\mathbf{K}_j\mathbf{u} = -\frac{2k}{\rho_j}C_j \tag{31}$$

where C_j is the compliance of the j^{th} element. Thus, Eq. (24) can be degraded into a scaling function similar to that used in size optimization as:

$$\frac{\partial C}{\partial \rho_j} = -\frac{1}{2}\mathbf{u}^T \frac{\partial \mathbf{K}_j}{\partial \rho_j}\mathbf{u} = -\frac{k}{\rho_j}C_j \tag{32}$$

Sensitivity of the volume fraction is calculated as:

$$\frac{\partial v_{\mathrm{F}}}{\partial \rho_j} = \frac{V_j}{V} \tag{33}$$

3.2 Sensitivities of the nested p-norm of Tsai-Hill failure indexes

For topology optimization involving a large number of design variables, sensitivities are calculated using the adjoint method by solving the adjoint problem under the same FE formulation of the original problem. The same strategy is used here for deriving the stress sensitivities.

Sensitivities of the nested p-norm of the failure indexes, as expressed in Eq. (10), are formulated as:

$$\frac{\partial F_{\mathrm{N}}}{\partial \rho_j} = \sum_{e=1}^{n_{\mathrm{E}}}\left(\frac{\partial F_{\mathrm{N}}}{\partial F_e}\sum_{i=1}^{n_{\mathrm{L}}}\left(\frac{\partial F_e}{\partial F_{\mathrm{TH}}^{\{i,e\}}}\frac{\partial F_{\mathrm{TH}}^{\{i,e\}}}{\partial \boldsymbol{\sigma}_*^{\{i,e\}}}\frac{\partial \boldsymbol{\sigma}_*^{\{i,e\}}}{\partial \rho_j}\right)\right) \tag{34}$$

where the first three items on the right hand side are expressed as:

$$\frac{\partial F_{\mathrm{N}}}{\partial F_e} = \left(\frac{F_{\mathrm{N}}}{F_e}\right)^{1-p} \tag{35}$$

$$\frac{\partial F_e}{\partial F_{\mathrm{TH}}^{\{i,e\}}} = \left(\frac{F_e}{F_{\mathrm{TH}}^{\{i,e\}}}\right)^{1-q} \tag{36}$$

$$\frac{\partial F_{\mathrm{TH}}^{\{i,e\}}}{\partial \boldsymbol{\sigma}_*^{\{i,e\}}} = 2\boldsymbol{\sigma}_*^{\{i,e\}}\mathbf{M}_{\mathrm{TH}} \tag{37}$$

through derivations of Eqs. (16), (17) and (10), respectively.

According to Eqs. (8) and (9), the stress vector in the local coordinate system, denoted by $\boldsymbol{\sigma}_*^{\{i,e\}}$, for the e^{th} element at the i^{th} layer is formulated as:

$$\boldsymbol{\sigma}_*^{\{i,e\}} = \rho_e^s \mathbf{Q}_0 \mathbf{T}_i^T \mathbf{B}_e \mathbf{L}_e \mathbf{u} \tag{38}$$

where the superscript $\{i,e\}$ denotes the quantities of the e^{th} element at the i^{th} layer, the subscript * denotes the items obtained at the local 1-2 coordinate system; $\mathbf{T}_i$ is the rotation matrix of the i^{th} layer; $\mathbf{L}_e$ is the index matrix of the e^{th} element to extract its displacement components; $\mathbf{B}_e$ is the strain-displacement matrix for the e^{th} element; and the exponent s on the projected density of ρ_e denotes the *qp* relaxation factor for intermediate densities to avoid the stress singularity (with s=0.5 in this work). Thus, sensitivity of the local stresses is calculated as:

$$\frac{\partial \boldsymbol{\sigma}_*^{\{i,e\}}}{\partial \rho_j} = s\rho_e^{s-1}\frac{\partial \rho_e}{\partial \rho_j}\mathbf{Q}_0 \mathbf{T}_i^T \mathbf{B}_e \mathbf{L}_e \mathbf{u} + \rho_e^s \mathbf{Q}_0 \mathbf{T}_i^T \mathbf{B}_e \mathbf{L}_e \frac{\partial \mathbf{u}}{\partial \rho_j} \tag{39}$$

It is pointed out here that, $\frac{\partial \rho_e}{\partial \rho_j} \neq 0$, is only valid when e=j. By substituting Eq. (30) and recalling Eq. (38), Eq. (39) is rewritten as:

$$\frac{\partial \boldsymbol{\sigma}_*^{\{i,e\}}}{\partial \rho_j} = \frac{\partial \rho_e}{\partial \rho_j}\frac{s}{\rho_e}\boldsymbol{\sigma}_*^{\{i,e\}} - \frac{k}{\rho_j}\rho_e^s \mathbf{Q}_0 \mathbf{T}_i^T \mathbf{B}_e \mathbf{L}_e \mathbf{K}^{-1}\mathbf{K}_j \mathbf{u} \tag{40}$$

By combining Eq. (30) with Eqs. (35-37), Eq. (34) for sensitivity calculation of the obtained nested p-norm is rewritten as:

$$\begin{aligned}\frac{\partial F_{\mathrm{N}}}{\partial \rho_j} &= 2\sum_{e=1}^{n_{\mathrm{E}}}\left\{\left(\frac{F_{\mathrm{N}}}{F_e}\right)^{1-p}\sum_{i=1}^{n_{\mathrm{L}}}\left[\left(\frac{F_e}{F_{\mathrm{TH}}^{\{i,e\}}}\right)^{1-q}\left(\boldsymbol{\sigma}_*^{\{i,e\}}\right)^T \mathbf{M}_{\mathrm{TH}}\frac{\partial \boldsymbol{\sigma}_*^{\{i,e\}}}{\partial \rho_j}\right]\right\}\\ &= \frac{2(F_{\mathrm{N}})^{1-p}}{\rho_j}\left\{s\left(F_j\right)^{p-q}\sum_{i=1}^{n_{\mathrm{L}}}\left(F_{\mathrm{TH}}^{\{i,j\}}\right)^q\right.\\ &\left.- k\sum_{e=1}^{n_{\mathrm{E}}}\left[\rho_e^s (F_e)^{p-q}\sum_{i=1}^{n_L}\left(\left(F_{\mathrm{TH}}^{\{i,e\}}\right)^{q-1}\left(\boldsymbol{\sigma}_*^{\{i,e\}}\right)^T \mathbf{M}_{\mathrm{TH}}\mathbf{Q}_0\mathbf{T}_i^T\mathbf{B}_e\mathbf{L}_e\right)\right]\mathbf{K}^{-1}\mathbf{K}_j\mathbf{u}\right\}\end{aligned} \tag{41}$$

with a simplification form after reorganization:

$$\begin{aligned}\frac{\partial F_{\mathrm{N}}}{\partial \rho_j} &= \frac{2(F_{\mathrm{N}})^{1-p}}{\rho_j}\left(s\left(F_j\right)^{p-q}\sum_{i=1}^{n_{\mathrm{L}}}\left(F_{\mathrm{TH}}^{\{i,j\}}\right)^q - k\boldsymbol{\lambda}^T\mathbf{K}_j\mathbf{u}\right)\\ &= \frac{2(F_{\mathrm{N}})^{1-p}}{\rho_j}\left(s\left(F_j\right)^p - k\boldsymbol{\lambda}^T\mathbf{K}_j\mathbf{u}\right)\end{aligned} \tag{42}$$

where the adjoint variable $\boldsymbol{\lambda}$ is calculated by solving the following adjoint problem:

$$\mathbf{K}\boldsymbol{\lambda} = \sum_{e=1}^{n_E}\rho_e^s (F_e)^{p-q}\sum_{i=1}^{n_L}\left(\left(F_{\mathrm{TH}}^{\{i,e\}}\right)^{q-1}\left(\mathbf{Q}_0\mathbf{T}_i^T\mathbf{B}_e\mathbf{L}_e\right)^T\mathbf{M}_{\mathrm{TH}}\boldsymbol{\sigma}_*^{\{i,e\}}\right) \tag{43}$$

The above adjoint problem can be solved by recalling the original equilibrium expression of Eq. (25). With the substitution of the adjoint variable, as expressed in Eq. (43), into Eq. (42), and integrated with the filtered projected density sensitivity expressed in Eq. (21), the semi-analytical sensitivity of the nested p-norm for the Tsai-Hill failure indexes is obtained.

4. Case studies

In this section, four typical two-dimensional examples with stress concentrations, i.e., an L-shaped bracket, a crack problem for a square plate with intermediate notch, a corbel structure, and an antenna support bracket, are used to validate the effectiveness of the proposed nested p-norm method for topology optimization in DD laminates considering stress control. The composite parameters are listed as: E_1=140.8 GPa, E_2=9.3 GPa, ν_{12}=0.3, G_{12}=5.8 GPa, X=2.944 GPa, Y=66 MPa, S=93 MPa. In the optimization, the filtering radius r_0 used in Eq. (A1) and Figure A2 is set to be 3.2 times of the average element size while the projection parameter η in Eq. (A3) is equal to 0.3 in order to reduce relatively thin structural details in the optimized structure. The initial value of β is chosen as 1. For each 50 iterations, β would be doubled until it reaches 32.

For each case, the same geometry under the same loading condition and the same volume fraction constraint of v_f=0.5 are used for investigation. Both DD and Quad laminates with the layups of $[\pm 68^{\circ}/\pm 22^{\circ}]_4$ and $[0^{\circ}/90^{\circ}/\pm 45^{\circ}]_{2s}$ are included with the equivalent Quasi-Isotropic (QI) stiffness for comparison. For the first three examples, the optimal solutions using the one p-norm and the layer-wise p-norm are also provided together with the proposed nested p-norm method for DD laminates with QI stiffness to investigate the differences in optimal solutions using different p-norm methods.

At the same time, two additional typical DD laminate layups of $[\pm 0^{\circ}/\pm 50^{\circ}]_4$, and $[\pm 32^{\circ}/\pm 58^{\circ}]_4$ representing hard and soft stiffness and two other DD laminate layups of $[\pm 45^{\circ}]_8$ and $[0^{\circ}/90^{\circ}]_8$ as a single double and its rotation, which is also a special DD, are included to investigate the influence of laminate layups for all the four examples. It is noticeable that all the figures of stress distributions provided for DD laminates are using the ply sequences of $[\Phi/\text{-}\Psi/\text{-}\Phi/\Psi]$ for illustration.

Moreover, optimal topologies for isotropic materials are also provided as a comparison for the first example. Material parameters for the isotropic material are listed as: E=120GPa, v=0.31, X=862MPa.

4.1 An L-shaped bracket

L-shaped bracket is a typical test example for stress-constrained topology optimization using isotropic material [33,39]. As illustrated in Figure 6, an L-shaped bracket with a length of 100 mm, and a thickness of 1 mm is used here. The design domain is discretized into 6400 equal elements with the upper left end fixed. A vertical downward load of 800 N is distributed to the adjacent nodes of the right top corner, to avoid the stress concentration at the loading point.

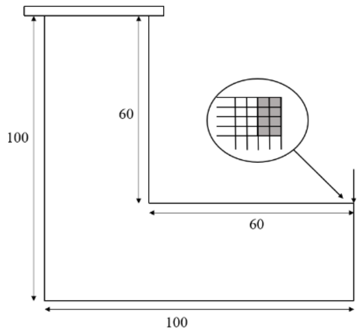

Figure 6. Design domain and boundary conditions of an L-shaped bracket.

The optimal topology and the distribution of the Tsai-Hill failure indexes for the L-shaped bracket with a DD layup of $[\pm 68^{\circ}/\pm 22^{\circ}]_4$ are provided in Figure 7(b). This DD layup has an equivalent stiffness as the QI Quad with the layup of $[0^{\circ}/90^{\circ}/\pm 45^{\circ}]_{2s}$ [71]. The proposed nested p-norm method is used to minimize the maximum of the Tsai-Hill failure indexes by using the optimization model in Eq. (18). The elemental failure indexes for each layer and the maximum value through the thickness, denoted by $\max(F^{\{i,e\}})$, are all provided in Figure 7. As a comparison, the optimal results without stress control using the optimization model in Eq. (19) are provided in Figure 7(a).

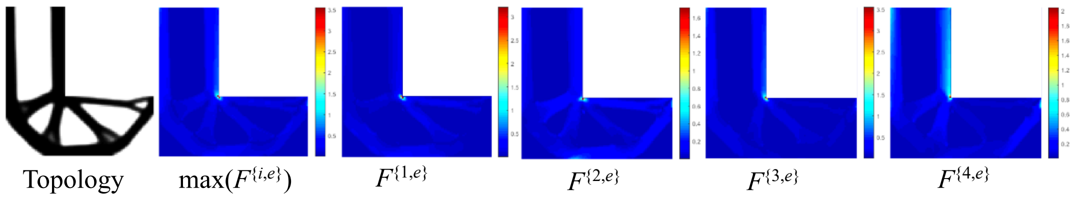

(a) Without stress control, v_f=0.5, C=2167, $\max(F^{\{i,e\}})$=3.552

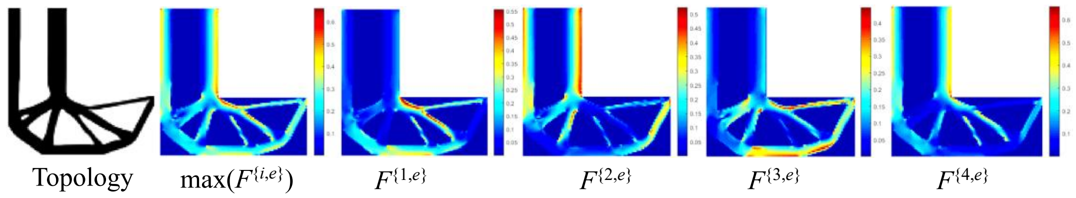

(b) With stress control, v_f=0.5, C=2351, $\max(F^{\{i,e\}})$=0.661

Figure 7. The optimal topology and the distribution of the Tsai-Hill failure indexes of the L-shaped bracket with a DD layup of $[\pm 68^{\circ}/\pm 22^{\circ}]_{2s}$ using the proposed nested p-norm method (with C denoting compliance, v_f denoting the volume fraction, and $F^{\{i,e\}}$ denoting the Tsai-Hill failure index of the e^{th} element in the i^{th} layer).

It is shown that using the proposed nested p-norm method can effectively reduce the stress concentration in DD laminates with a reduction of 81% for the maximum Tsai-Hill failure index. The resulting optimal topology has a groove at the corner of the L-shape. The purpose of reducing stress concentration is achieved by digging out the material at the corner. This optimal configuration is similar to that obtained from topology optimization for a Quad layup with the equivalent QI stiffness, and isotropic material, as illustrated in Figures 8 and 9, respectively. It is noted that there are some differences in the details of the optimal configurations.

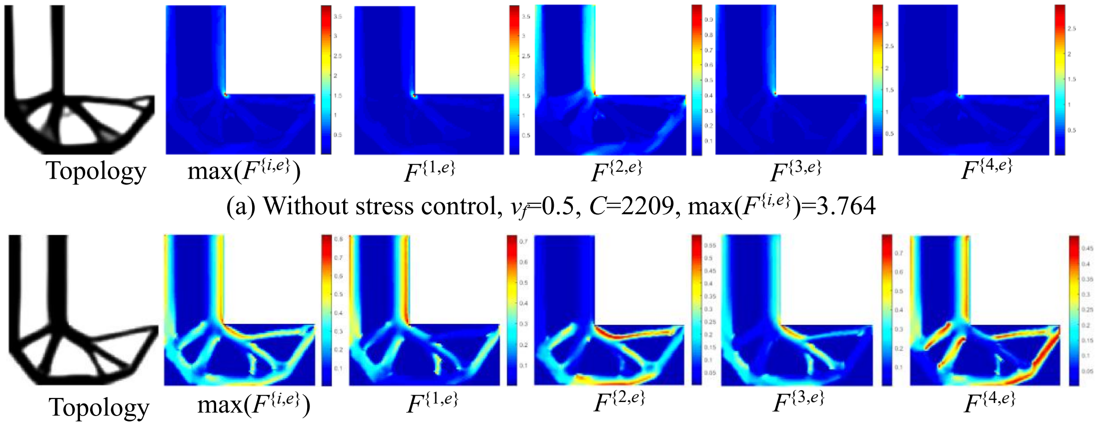

(a) Without stress control, v_f=0.5, C=2209, $\max(F^{\{i,e\}})$=3.764

(b) With stress control, V_f=0.5, C=2732, $\max(F^{\{i,e\}})$=0.822

Figure 8. The optimal topology and the distribution of the Tsai-Hill failure indexes of the L-shaped bracket with a Quad layup of $[0°/90°/\pm45°]_{2s}$ using the proposed nested p-norm method.

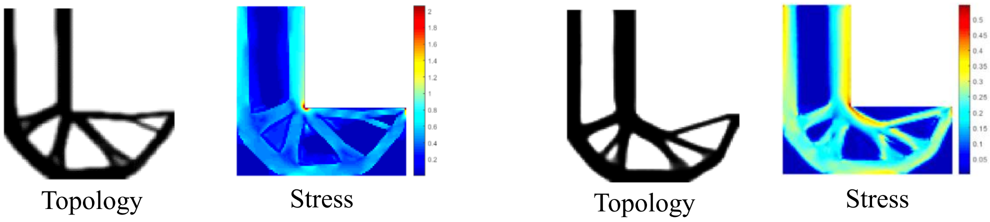

(a) Without stress control

(b) With stress control

Figure 9. Topology optimization results of a L-shaped bracket made of isotropic materials.

At the same time, the optimization results by using the one p-norm method and the layer-wise p-norm method are provided in Figures 10 and 11. Both the one p-norm method and the layer-wise p-norm method lead to a larger Tsai-Hill failure index. The optimized structure obtained from the one p-norm method still has obvious local stress concentrations. In addition, compared with the nested p-norm method, the optimized configurations obtained by the other two methods have more difficult converging.

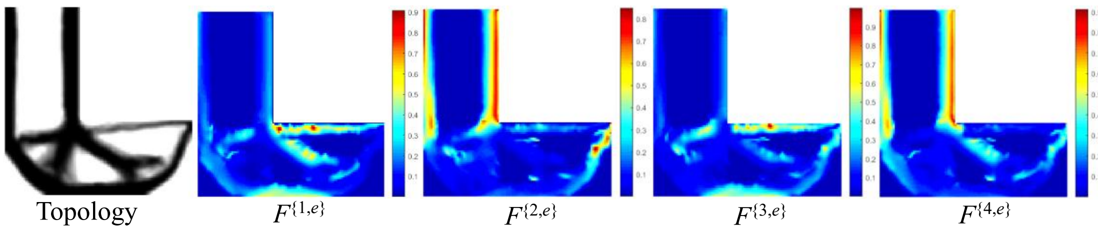

Figure 10. The distribution of the Tsai-Hill failure indexes for the optimal L-shaped bracket with a DD layup of $[\pm68/\pm22]_4$ using the one p-norm method with v_f=0.5, C=2830, and $\max(F^{\{i,e\}})$=0.999.

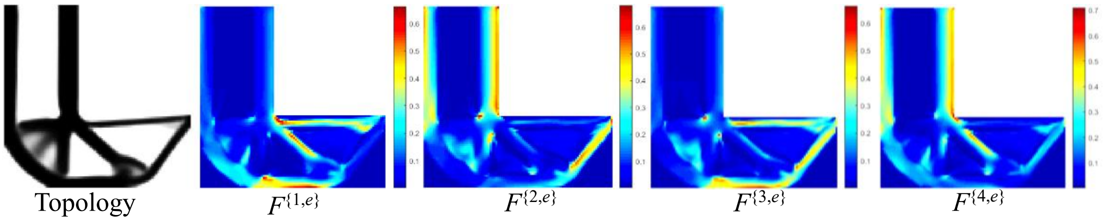

Figure 11. The distribution of the Tsai-Hill failure indexes for the optimal L-shaped bracket with a DD layup of $[\pm 68/\pm 22]_4$ using the layer-wise p-norm method with v_f=0.5, C=2543, and $\max(F^{\{i,e\}})$=0.709.

To investigate the influence of laminate layups on the optimal configuration and the optimization effects, four different DD layups with two representing hard and soft, respectively, (i.e., $[\pm 0^{\circ}/\pm 50^{\circ}]_4$ and $[\pm 32^{\circ}/\pm 58^{\circ}]_4$) and two representing a soft single DD and its rotation (i.e., $[\pm 45^{\circ}]_8$ and $[0^{\circ}/90^{\circ}]_8$), which are special DDs, are optimized using the proposed nested p-norm method. The results obtained after optimization are summarized in Table 1 and the optimal structure and the distribution of the maximum elemental Tsai-Hill failure indexes are illustrated in Figures 12-15. By comparing with the optimization results without considering the stress control, the proposed nested p-norm can effectively reduce the stress concentrations of laminated structures with different layups. As illustrated in Figures 12 and 13, the reductions of the stress concentration are 70% and 60% for the layups of $[\pm 45^{\circ}]_8$ and $[0^{\circ}/90^{\circ}]_8$, respectively. As illustrated in Figures 14-15, the reductions of the stress concentration are 69% and 78% for the layups of $[\pm 0^{\circ}/\pm 50^{\circ}]_4$ and $[\pm 32^{\circ}/\pm 58^{\circ}]_4$, respectively. The results show the effectiveness of the proposed method, and at the same time, the optimization results show that the optimized configuration has a strong correlation with the laminate layup.

Table 1 Comparison of the optimal results for an L-shaped bracket with different DD angles.

Laminate	Layup	p-norm	max(F{i,e}) No Stress control	max(F{i,e}) Stress control	Reduction
Isotropic	/	One	2.256	0.541	76%
Quad	$[0^{\circ}/90^{\circ}/\pm 45^{\circ}]_{2s}$	Nest	3.764	0.822	78%
DD	$[\pm 68^{\circ}/\pm 22^{\circ}]_4$	One	3.553	0.999	72%
		Layer-wise	3.553	0.709	80%
		Nest	3.553	0.661	81%
	$[\pm 0^{\circ}/\pm 50^{\circ}]_4$	Nest	6.321	1.983	69%
	$[\pm 32^{\circ}/\pm 58^{\circ}]_4$	Nest	4.882	1.084	78%
	$[\pm 45^{\circ}]_8$	Nest	10.34	3.084	70%
	$[0^{\circ}/90^{\circ}]_8$	Nest	3.928	1.568	60%

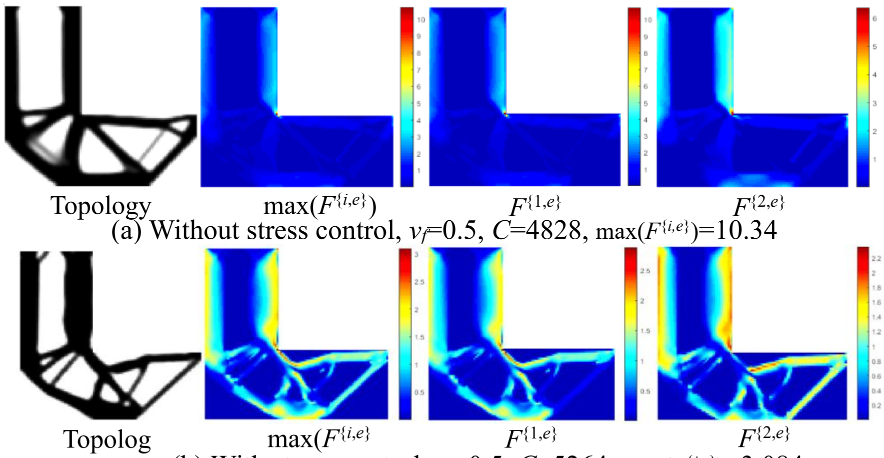

(a) Without stress control, v_f=0.5, C=4828, $\max(F^{\{i,e\}})$=10.34

(b) With stress control, v_f=0.5, C=5264, $\max(F^{\{i,e\}})$=3.084

Figure 12. Topology optimization results and the distribution of Tsai-Hill failure index for composite L-shaped bracket with the layup of [±45°]$_8$.

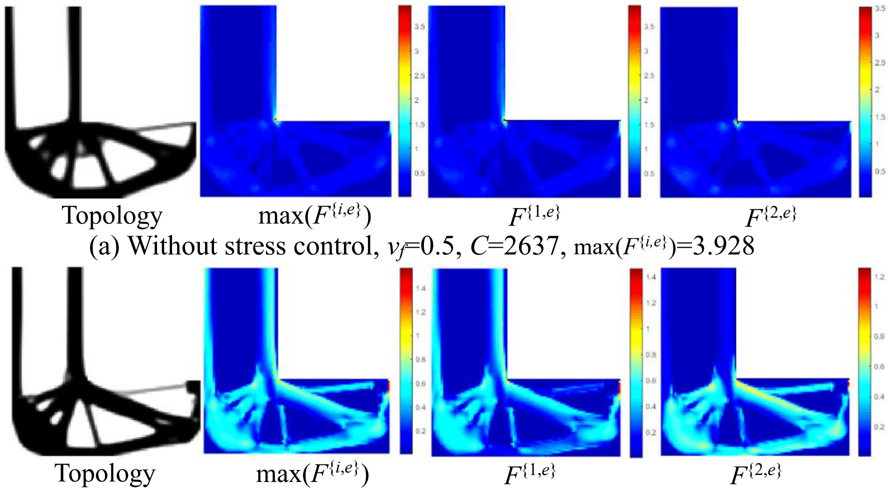

(a) Without stress control, v_f=0.5, C=2637, max($F^{\{i,e\}}$)=3.928

(b) With stress control, v_f=0.5, C=3011, max($F^{\{i,e\}}$)=1.568

Figure 13. Topology optimization results and strength index distribution of composite L-shaped bracket with the layup of [0°/90°]$_8$.

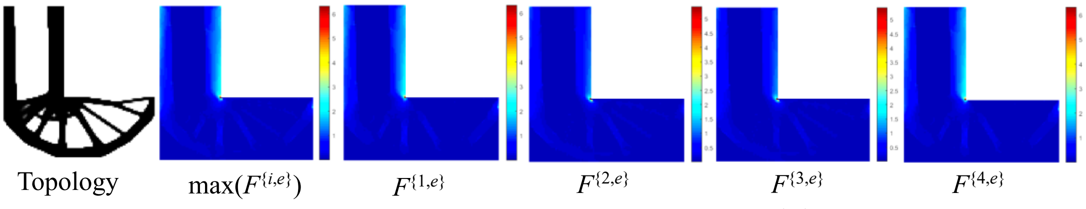

(a) Without stress control, v_f=0.5, C=2906, max($F^{\{i,e\}}$)=6.321

(b) With stress control, V_f=0.5, C=3726, max($F^{\{i,e\}}$)=1.983

Figure 14. Topology optimization results and strength index distribution of composite L-shaped bracket with the layup of [±0°/±50°]$_4$.

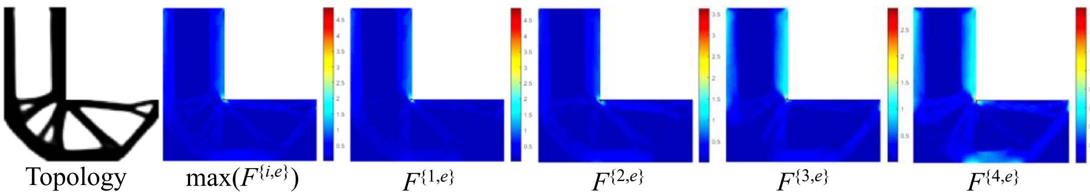

(a) Without stress control, v_f=0.5, C=2817, max($F^{\{i,e\}}$)=4.882

(b) With stress control, V_f=0.5, C=3033, max($F^{\{i,e\}}$)=1.084

Figure 15. Topology optimization results and strength index distribution of composite L-shaped bracket with the layup of [±32°/±58°]$_4$.

4.2 A crack problem

As illustrated in Figure 16(a), a crack problem is considered here for a square plate with an intermediate notch under tensile load. The dimension and load are defined as L=100 *mm*, P=800 *N,* respectively. To improve the calculational efficiency, half of the structure is used for calculation due to the structural sysmmetry (Figure 16(b)). Symmetric boundary conditions are added at the lower part of the left boundary, and a horizontal load is applied to the upper right corner. As illustrated in Figure 16(c), a large stress concentration exists at the crack tip of the structure with solid laminate materials.

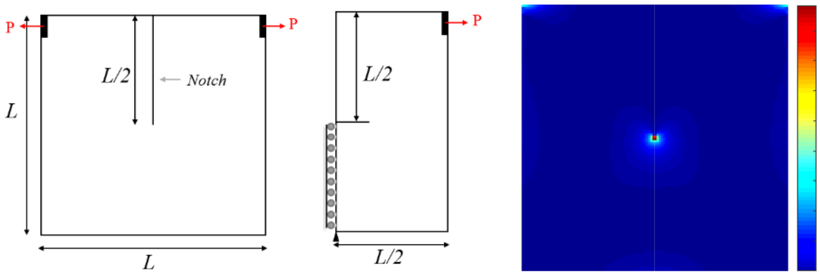

(a) Full model (b) Half model (c) Tsai-Hill failure indexes

Figure 16. Design domain, boundary conditions and the stress concentration for a square plate with an intermediate notch under tensile load.

The optimal topology and the distribution of the Tsai-Hill failure indexes for the half model of tensile square plate with a DD layup of [±68°/±22°]$_4$ are provided in Figure 17(b). The proposed nested p-norm method is used to minimize the Tsai-Hill failure index by using the optimization model of Eq. (18). Meanwhile, the optimal results without stress control using the optimization model of Eq. (19) are provided in Figure 17(a). It is shown that there is a high stress concentration at the notch tip of the DD laminate structure, and it is effectively relieved with a reduction of 69% when the stress control is implemented during optimization. The optimized structure digs out more material at the crack tip of the previous solid structure, as shown in Figure 16, and provides a smooth transition structure at the new crack tip position, thereby eliminating the big stress concentration at the crack tip of the previous structure. This optimal configuration is similar to that obtained from topology optimization for a QI Quad layup with the equivalent stiffness, as illustrated in Figure 18.

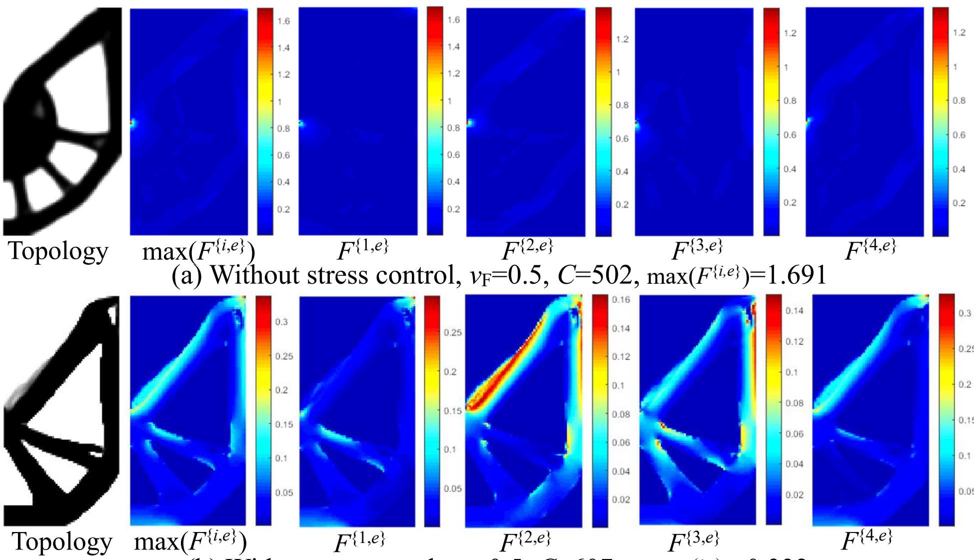

(a) Without stress control, v_F=0.5, C=502, $\max(F^{\{i,e\}})$=1.691

(b) With stress control, v_F=0.5, C=607, $\max(F^{\{i,e\}})$=0.332

Figure 17. The distribution of the Tsai-Hill failure indexes of the optimal square plate with an intermediate notch with a DD layup of [±68°/±22°]$_4$ using the proposed nested p-norm method.

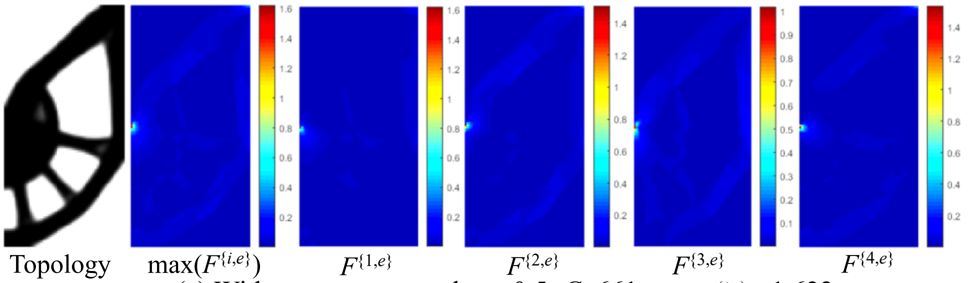

(a) Without stress control, v_F=0.5, C=661, max($F^{\{i,e\}}$)=1.622

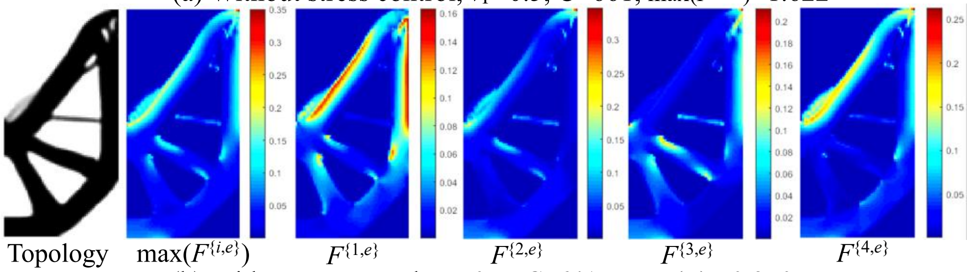

(b) With stress control, v_F=0.5, C=641, max($F^{\{i,e\}}$)=0.350

Figure 18. The distribution of the Tsai-Hill failure indexes of the optimal square plate with an intermediate notch with a Quad layup of [0°/90°/±45°]$_{2s}$ using the proposed nested p-norm method.

Optimal configurations and the distribution of the Tsai-Hill failure indexes obtained via single p-norm and layer-wise p-norm are provided in Figures 19 and 20, respectively. The solutions obtained using the single p-norm method failed to converge to a clear topology and exhibited a Tsai-Hill failure index that is 66% higher than that of the nested p-norm method. The layer-wise p-norm method provides a comparable optimal solution as the nested p-norm method. However, it was more difficult to achieve convergence and much longer optimization time was taken for the layer-wise p-norm method.

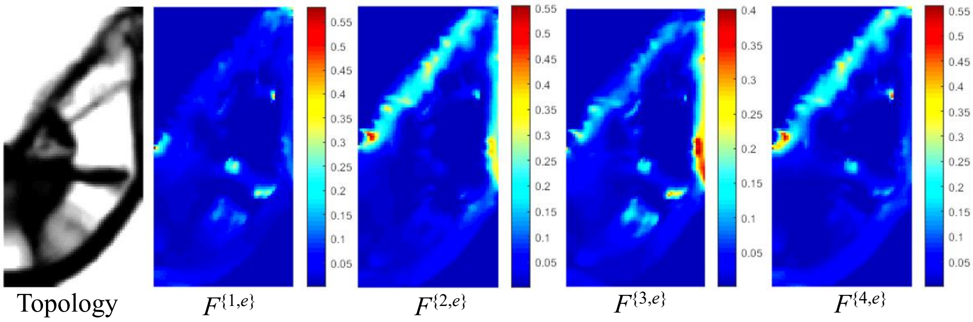

Figure 19. The distribution of the Tsai-Hill failure indexes of the optimal square plate with an intermediate notch with a DD layup of [±68°/±22°]$_4$ using the one p-norm method with v_F=0.5, C=816, max($F^{\{i,e\}}$)=0.582.

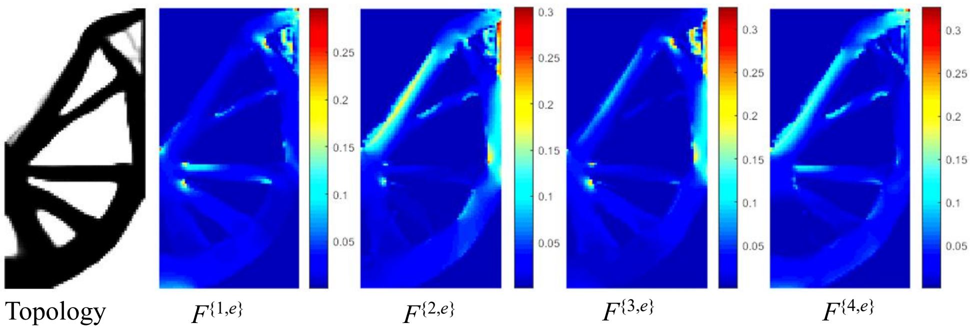

Figure 20. The distribution of the Tsai-Hill failure indexes of the optimal square plate with an intermediate notch with a DD layup of [±68º/±22º]$_4$ using the layer-wise p-norm method v_F=0.5, C=614, max($F^{\{i,e\}}$)=0.341.

To investigate the influence of the laminate layups and also to validate the effectiveness of the proposed nested p-norm method, four different DD layups with two representing hard and soft (i.e., [±0º/±50º]$_4$ and [±32º/±58º]$_4$), respectively, and two representing a soft single DD and its rotation (i.e., [±45º]$_8$ and [0º/90º]$_8$), which are special DDs, are optimized using the proposed nested p-norm method. The results obtained after optimization are summarized in Table 2 and the optimal structure and the distribution of the maximum elemental Tsai-Hill failure indexes are illustrated in Figures 21-24. For the structure with a stacking sequence of [0º/90º]$_8$, the stress concentration has been reduced by 80%, comparing with the optimization results without stress control. For the layup of [±45º]$_8$, the stress concentration still exists at the loading corner for the optimal configuration after optimization with stress control, though a smaller reduction of 36% was achieved. The reduction in stress concentration is 76% and 60% for layups of [±0º/±50º]$_4$ and [±32º/±58º]$_4$, respectively. Similar to the layup of [±45º]$_8$, the stress concentration is largely reduced, but still exist in the soft laminate with the layup of [±32º/±58º]$_4$ after optimization. All these results well validate the effectiveness of the proposed nested p-norm method in reducing the stress concentration of laminate structures.

Table 2 Comparison of the optimal results for a crack problem with different DD angles.

Laminate	Layup	p-norm	max($F^{\{i,e\}}$)		
			No stress control	Stress control	Reduction
Quad	[0°/90°/±45°]$_{2s}$	Nest	1.622	0.350	78%
DD	[±68°/±22°]$_4$	One	1.691	0.582	65%
		Layer-wise	1.691	0.347	79%
		Nest	1.691	0.332	81%
	[±0°/±50°]$_4$	Nest	1.812	0.452	76%
	[±32°/±58°]$_4$	Nest	1.712	0.672	60%
	[±45º]$_8$	Nest	1.794	1.151	36%
	[0º/90º]$_8$	Nest	2.794	0.569	80%

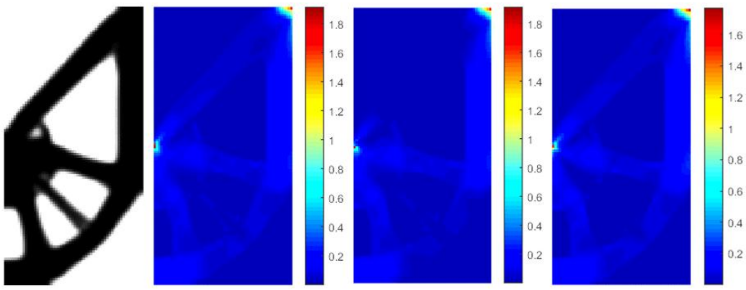

(a) Without stress control, v_F=0.5, C=740, max($F^{\{i,e\}}$)=1.794

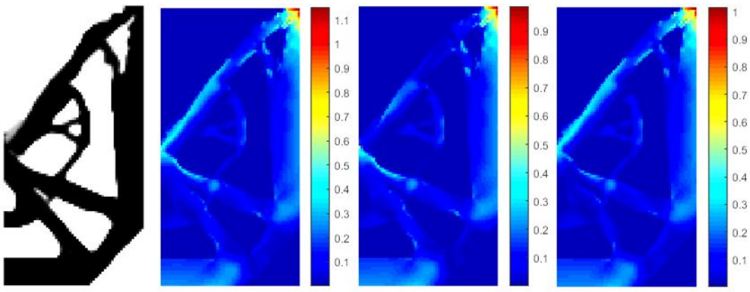

(b) With stress control, v_F=0.5, C=959, max($F^{\{i,e\}}$)=1.151

Figure 21. The distribution of the Tsai-Hill failure indexes of the optimal tensile square plate with an intermediate notch with a DD layup of $[\pm 45^{o}]_8$ using the nested p-norm method.

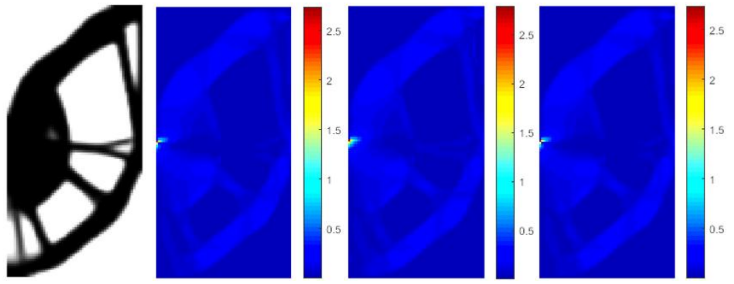

Topology max($F^{\{i,e\}}$) $F^{\{1,e\}}$ $F^{\{1,e\}}$

(a) Without stress control, v_F=0.5, C=864, max($F^{\{i,e\}}$)=2.794

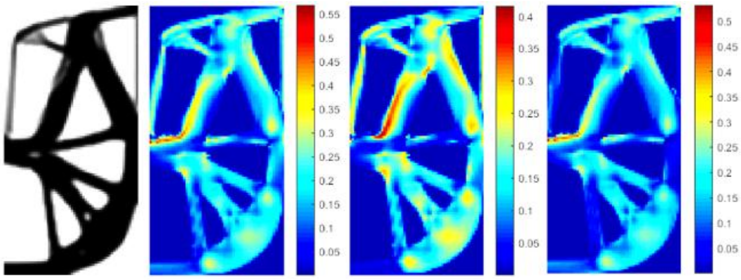

Topology max($F^{\{i,e\}}$) $F^{\{1,e\}}$ $F^{\{1,e\}}$

(b) With stress control, v_F=0.5, C=1135, max($F^{\{i,e\}}$)=0.569

Figure 22. The distribution of the Tsai-Hill failure indexes of the optimal tensile square plate with an intermediate notch with a DD layup of $[0^{o}/90^{o}]_8$ using the nested p-norm method.

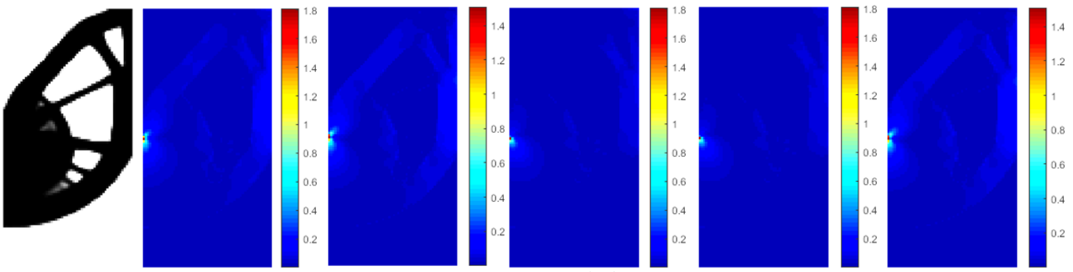

Topology max($F^{\{i,e\}}$) $F^{\{1,e\}}$ $F^{\{2,e\}}$ $F^{\{3,e\}}$ $F^{\{4,e\}}$

(a) Without stress control, v_F=0.5, C=542, max($F^{\{i,e\}}$)=1.812

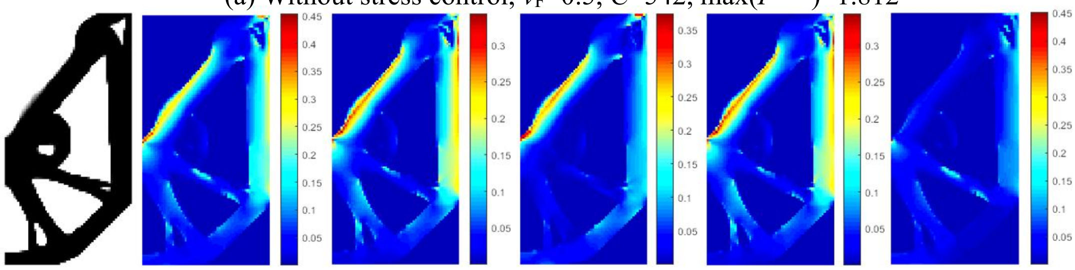

Topology max($F^{\{i,e\}}$) $F^{\{1,e\}}$ $F^{\{2,e\}}$ $F^{\{3,e\}}$ $F^{\{4,e\}}$

(b) With stress control, v_F=0.5, C=725, max($F^{\{i,e\}}$)=0.452

Figure 23. The distribution of the Tsai-Hill failure indexes of the optimal tensile square plate with an intermediate notch with a DD layup of $[\pm 0^{o}/\pm 50^{o}]_4$ using the nested p-norm method.

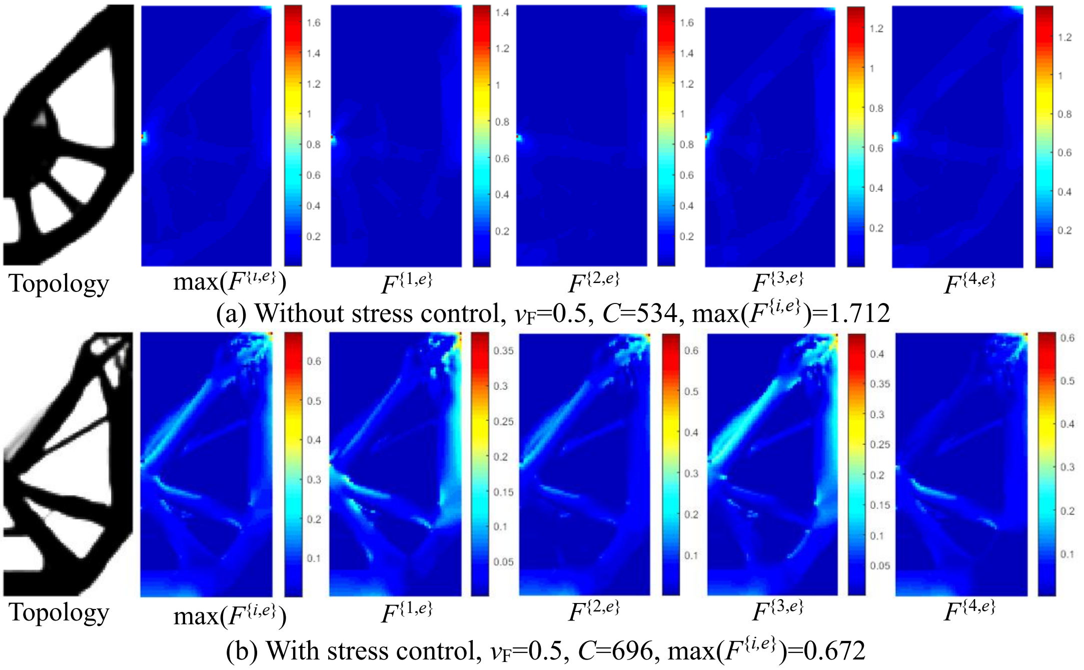

Figure 24. The distribution of the Tsai-Hill failure indexes of the optimal tensile square plate with an intermediate notch with a DD layup of [±32°/±58°]$_4$ using the nested p-norm method.

4.3 A corbel structure

A corbel structure is used here for validation. The load and boundary conditions are given in Figure 25. The force applied is 800 N and the unit for length is mm. Both the upper and lower ends are fixed and the load is applied on the right protruding part.

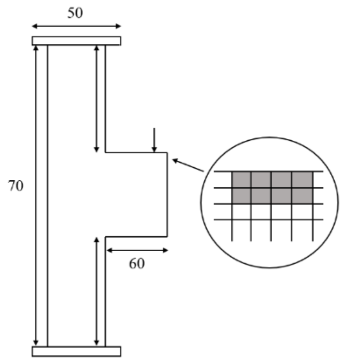

Figure 25. Geometry parameters of a corbel structure and its boundary conditions.

The optimal topology and the distribution of the Tsai-Hill failure indexes for the corbel model with a DD layup of [±68°/±22°]$_4$ are provided in Figure 26(b). It is shown that by using the proposed nested p-norm method, the maximum Tsai-Hill failure index has been reduced by 80%. Meanwhile, the optimal results without stress control using the optimization model of Eq. (19) are provided in Figure 26(a). It is shown that there is a high stress concentration at the two corners of the DD laminated structure. The groove at the top corner is similar as that in the optimal configuration of the L-shaped bracket. It is noticeable that the optimal configuration is unsymmetrical though starting from a symmetric geometry due to the unsymmetrical loading. At the same time, the optimal solution for a QI Quad layup with the equivalent stiffness is given in Figure 27. It is shown that DD and Quad with the equivalent QI stiffness have a similar optimal configuration with stress control. The maximum Tsai-Hill failure index is 61.8% higher for the Quad laminates than that of the DD ones, proving the advantage of DD laminates.

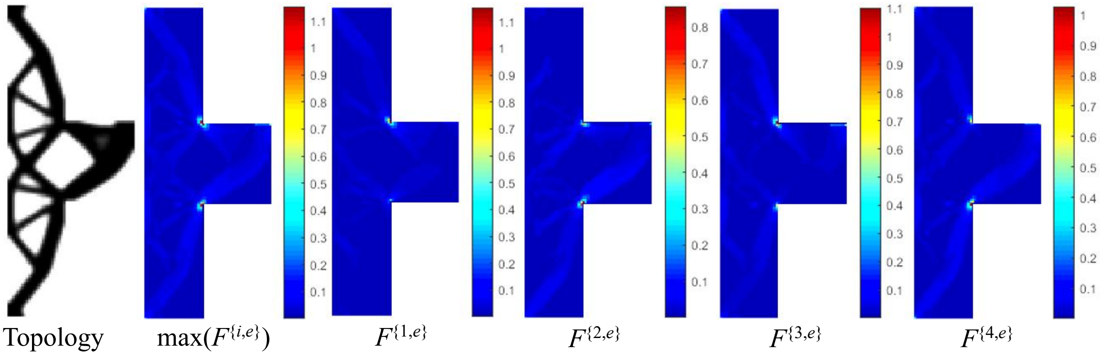

(a) Without stress control, v_F=0.5, C=344, max($F^{\{i,e\}}$)=1.151

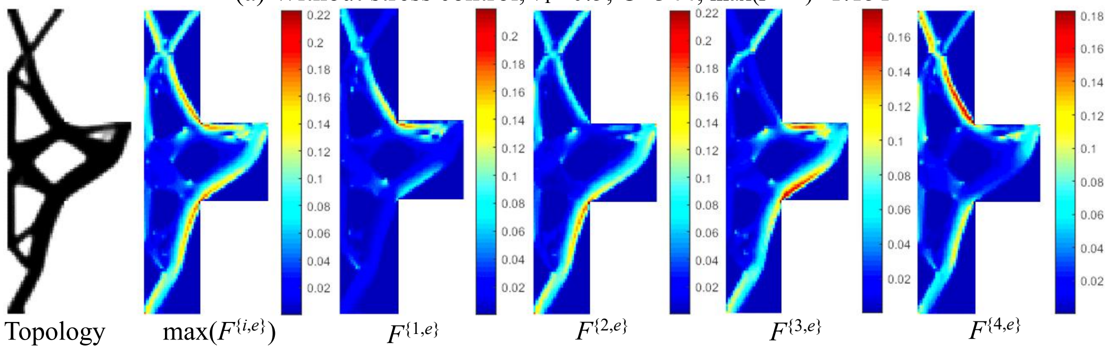

(b) With stress control, v_F=0.5, C=408, max($F^{\{i,e\}}$)=0.223

Figure 26. The distribution of the Tsai-Hill failure indexes of the optimal corbel structure with a DD layup of [±68°/±22°]$_4$ using the proposed nested p-norm method.

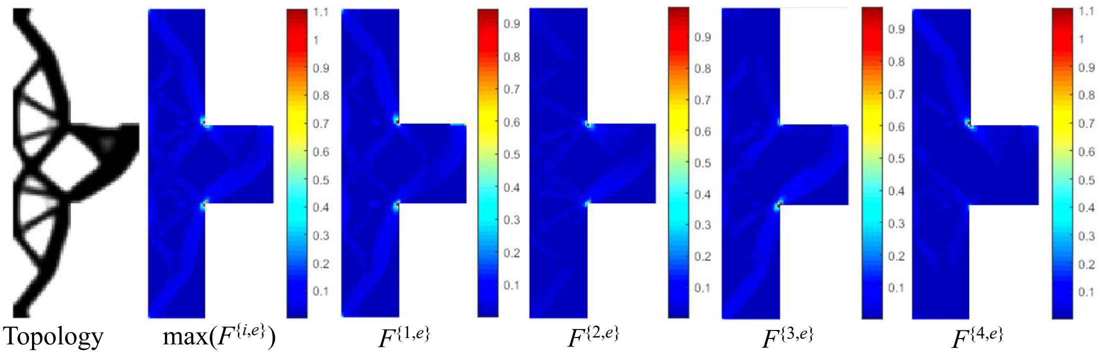

(a) Without stress control, v_F=0.5, C=327, max($F^{\{i,e\}}$)=1.108

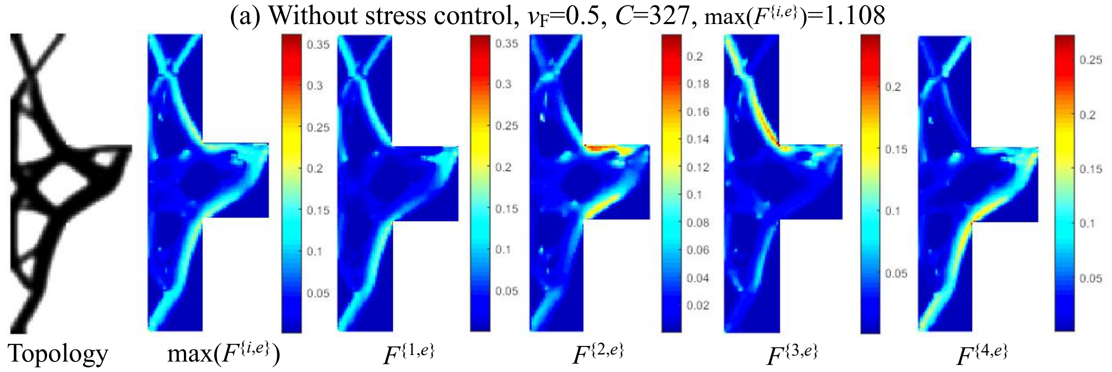

(b) With stress control, v_F=0.5, C=441, max($F^{\{i,e\}}$)=0.361

Figure 27. The distribution of the Tsai-Hill failure indexes of the optimal corbel structure with a Quad layup of [0°/90°/±45°]$_{2s}$ using the proposed nested p-norm method.

Optimization results obtained from using two other methods are also provided here in Figures 28 and 29. When the one p-norm method is used, obvious stress concentration exist at two corners and the optimal topology has a large number of intermediate pseudo densities. The layer-wise p-norm method leads to a better solution than that using one p-norm. However, the time taken by each step of sensitivity calculation is several times longer when compared with the nested p-norm method proposed in this study. Moreover, the computational time for the layer-wise p-norm method is linearly related to the number of representative plies. Additionally, more iteration steps are required for convergence when using the layer-wise p-norm method.

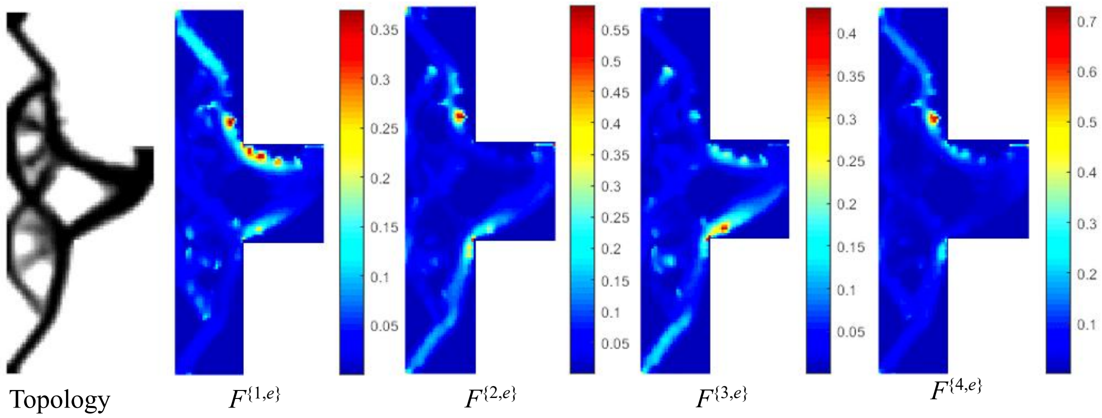

Figure 28. The distribution of the Tsai-Hill failure indexes of the optimal corbel structure with a DD layup of [±68°/±22°]$_4$ using the one p-norm method with v_F=0.5, C=478, max($F^{\{i,e\}}$)=0.728.

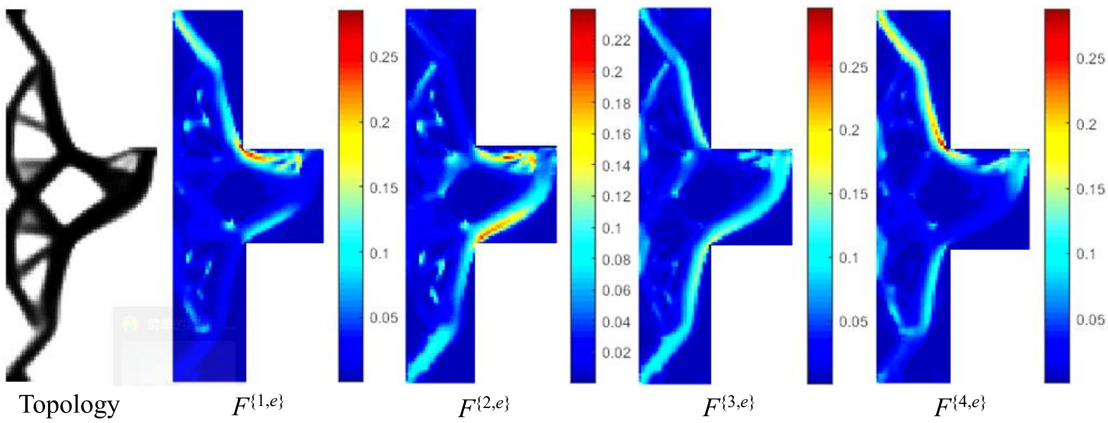

Figure 29. The distribution of the Tsai-Hill failure indexes of the optimal corbel structure with a DD layup of [±68°/±22°]$_4$ using the layer-wise p-norm method with v_F=0.5, C=426, max($F^{\{i,e\}}$)=0.297.

Table 3 Comparison of the optimal results for a corbel structure with different DD angles.

Laminate	Layup	p-norm	max($F^{\{i,e\}}$)		
			No Stress control	Stress control	Reduction
Quad	[0°/90°/±45°]$_{2s}$	Nest	1.108	0.361	67%
DD	[±68°/±22°]$_4$	One	1.151	0.728	37%
		Layer-wise	1.151	0.297	74%
		Nest	1.151	0.223	80%
	[±0°/±50°]$_4$	Nest	2.032	0.503	75%
	[±32°/±58°]$_4$	Nest	1.153	0.581	49%
	[±45°]$_8$	Nest	2.196	1.108	50%
	[0°/90°]$_8$	Nest	2.215	0.630	72%

The results obtained after optimization, including those of the other four DD laminates are summarized in Table 3 and the optimal structure as well as the distribution of the maximum elemental Tsai-Hill failure indexes are illustrated in Figures 30-33. The optimal results obtained via the one p-norm method and the layer-wise p-norm method both show less reductions in stress concentrations (37% and 74%, respectively), compared to the 80% of reduction by using the proposed nested p-norm method for the DD laminate with QI stiffness. The effect of layer-wise p-norm is close to the proposed method. However, as mentioned above, a largely increased computational time was observed. It is concluded that using the proposed nested p-norm method can significantly relieve the stress concentration on the laminated composite structures with a reduction of more than 49% after implementing stress control and the effectiveness is well validated from the optimal results with different DD layups of different stiffness.

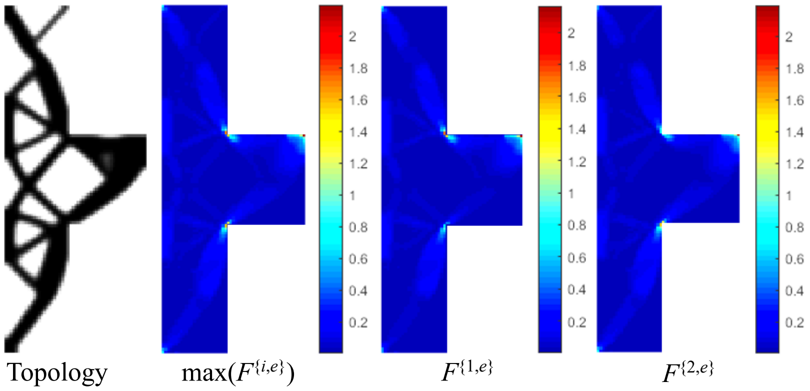

(a) Without stress control, v_F=0.5, C=467, max($F^{\{i,e\}}$)=2.196

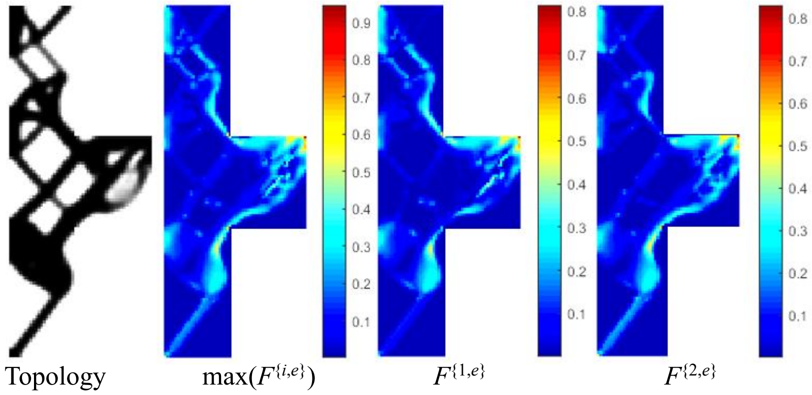

(b) With stress control, v_F=0.5, C=587, max($F^{\{i,e\}}$)=1.108

Figure 30. Optimization results and the distributions of Tsai-Hill failure indexes of a composite corbel structure with the layup of [±45]$_8$.

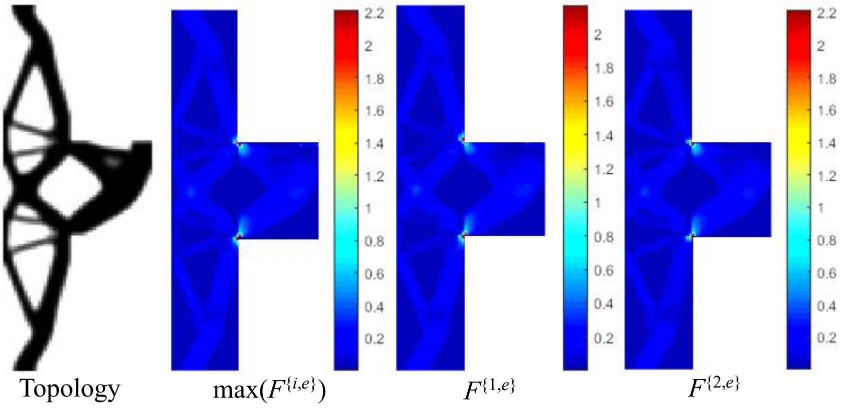

(a) Without stress control, v_F=0.5, C=607, max($F^{\{i,e\}}$)=2.215

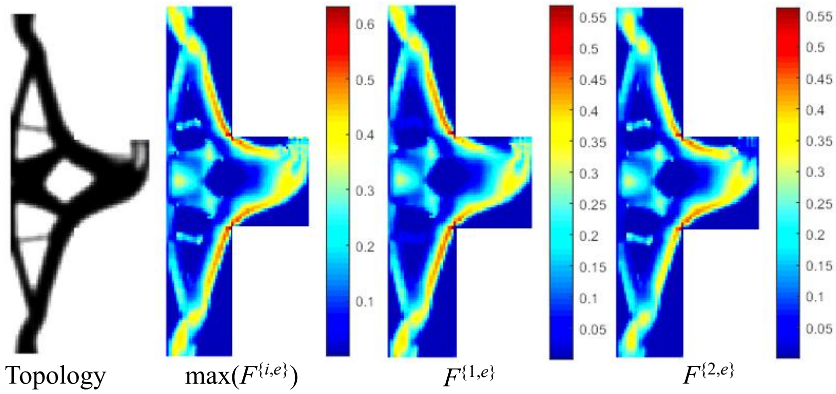

(b) With stress control, v_F=0.5, C=777, max($F^{\{i,e\}}$)=0.630

Figure 31. Optimization results and the distributions of Tsai-Hill failure indexes of a composite corbel structure with the layup of [0º/90º]$_8$.

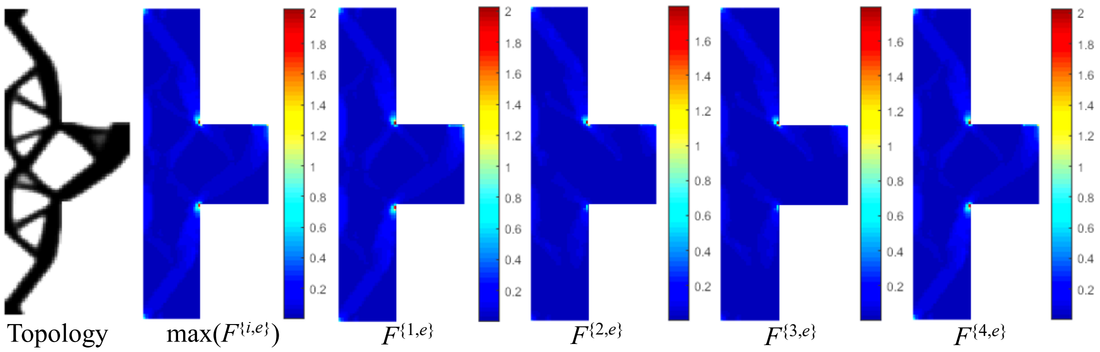

(a) Without stress control, v_F=0.5, C=409, max($F^{\{i,e\}}$)=2.032

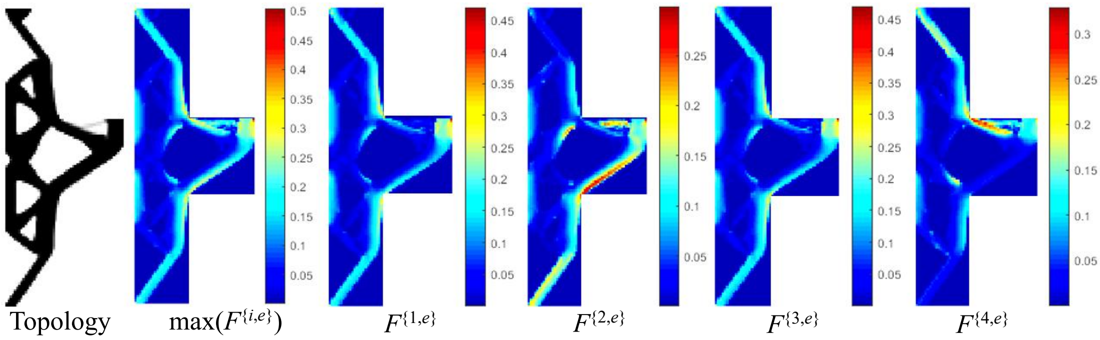

(b) With stress control, v_F=0.5, C=472, max($F^{\{i,e\}}$)=0.503

Figure 32. Optimization results and the distributions of Tsai-Hill failure indexes of a composite corbel structure with the layup of [±0º/±50º]$_4$.

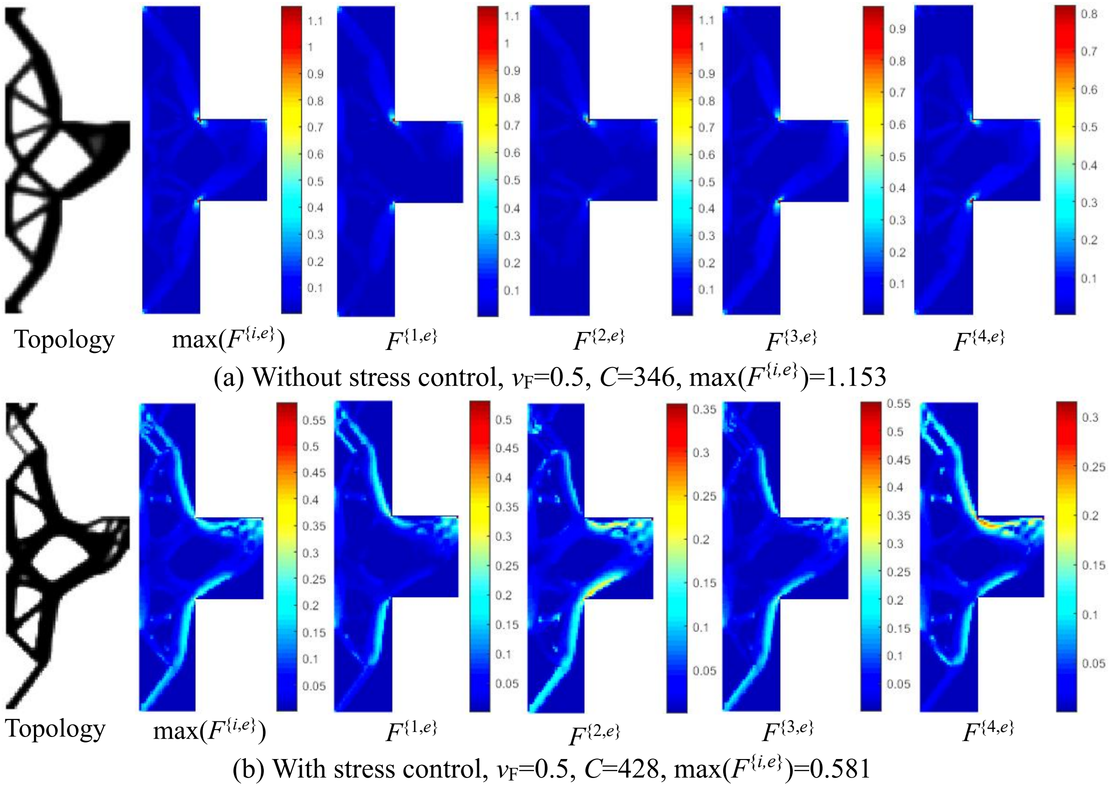

Figure 33. Optimization results and the distributions of Tsai-Hill failure indexes of a composite corbel structure with the layup of [±32°/±58°]$_4$.

4.4 An antenna support bracket

Here a model of an antenna support bracket [43] is used to simulate the industrial application of the optimized design of DD laminates. The geometry, the load and boundary conditions are illustrated in Figure 34. The parameters are defined as L=60 *mm*, H=105 mm, d=5 *mm* and P=800 *N*. The leftmost boundary is fixed, and the load is applied at the center of the upper bevel edge.

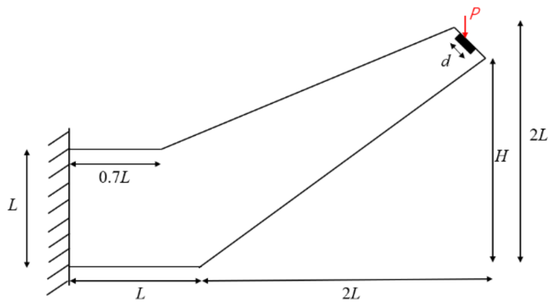

Figure 34. Schematic diagram of an antenna support bracket.

Firstly, a Quad laminate with the layup of [0°/90°/±45°]$_{2s}$ and a DD laminate with the layup of [±22°/±68°]$_4$ are used for comparison at the equivalent QI stiffness, as illustrated in Fig. 35 and 36, respectively. Secondly, optimized results for the other four DD laminates with the layups of [±0°/±50°]$_4$, [±32°/±58°]$_4$, [±45°]$_8$ and [0°/90°]$_8$ are also obtained. Relevant results are summarized in Table 4 and the optimal structures, and the distributions of the maximum elemental Tsai-Hill failure indexes are illustrated in Figures 35-40.

Both Quad and DD laminates with the layups of [0°/90°/±45°]$_{2s}$ and [±68°/±22°]$_4$, respectively, have an effective stress reduction of 67% for the maximum Tsai-Hill failure indexes, as seen in Figures 35 and 36, respectively, compared with those obtained from the compliance minimization optimization without stress control. Also seen from the optimization results for the laminates with other DD layups, stress concentrations have been reduced by more than 45% for all the DD layups.

These results validate the effectiveness of the proposed method and show the computational ability of the method for a more complex structure composed of laminated composites.

Table 4 Comparison of the optimal results for an antenna support bracket with different DD layups.

Laminate	Layup	p-norm	$\max(F^{\{i,e\}})$		
			No Stress control	Stress control	Reduction
Quad	$[0°/90°/\pm45°]_{2s}$	Nest	1.882	0.621	67%
DD	$[\pm68°/\pm22°]_4$	Nest	1.826	0.604	67%
	$[\pm0°/\pm50°]_4$	Nest	0.947	0.519	45%
	$[\pm32°/\pm58°]_4$	Nest	2.507	0.979	61%
	$[\pm45°]_8$	Nest	4.443	1.999	55%
	$[0°/90°]_8$	Nest	3.146	1.352	57%

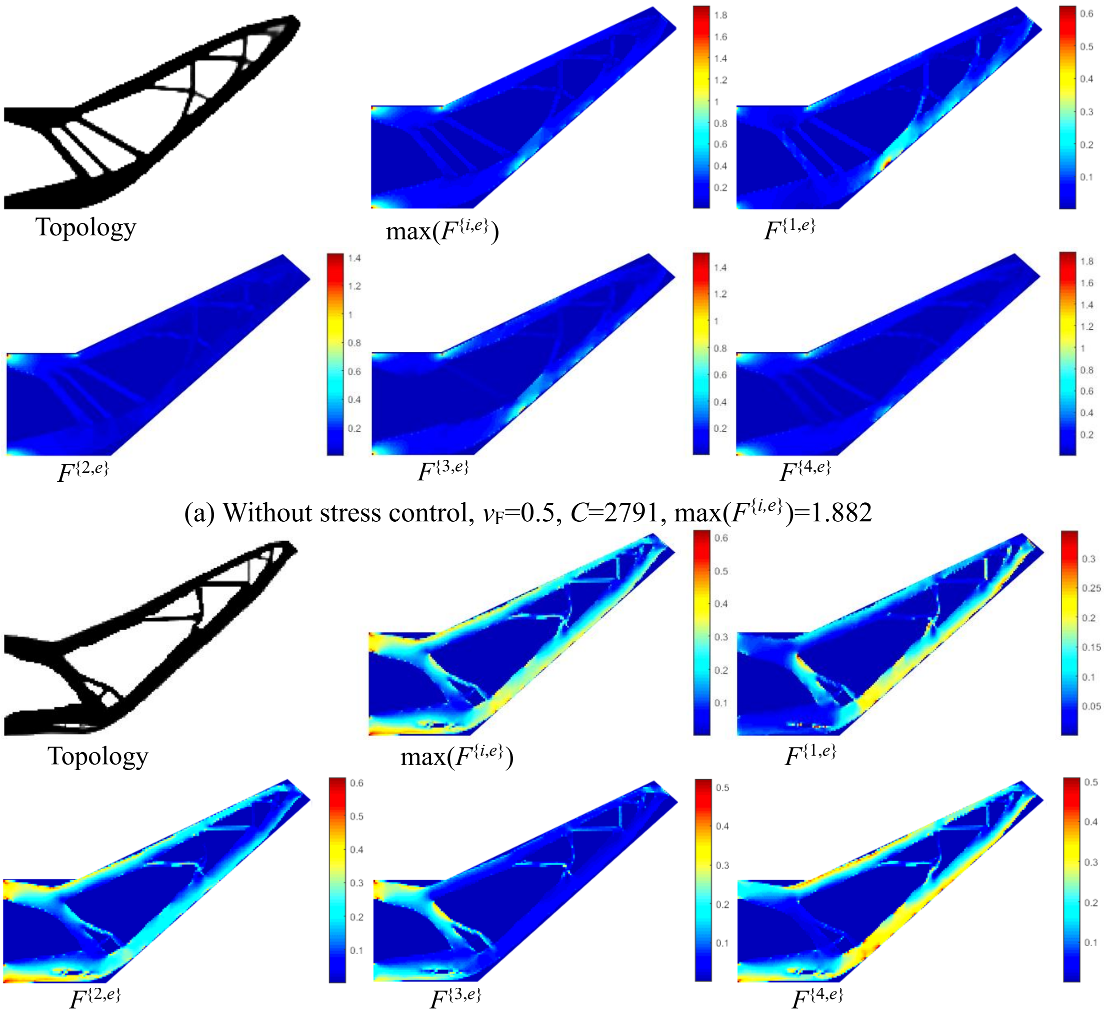

(a) Without stress control, v_F=0.5, C=2791, $\max(F^{\{i,e\}})$=1.882

(b) With stress control, v_F=0.5, C=3144, $\max(F^{\{i,e\}})$=0.621

Figure 35. The distribution of the Tsai-Hill failure indexes of the optimal antenna support bracket with a DD layup of $[0°/90°/\pm45°]_{2s}$ using the proposed nested p-norm method.

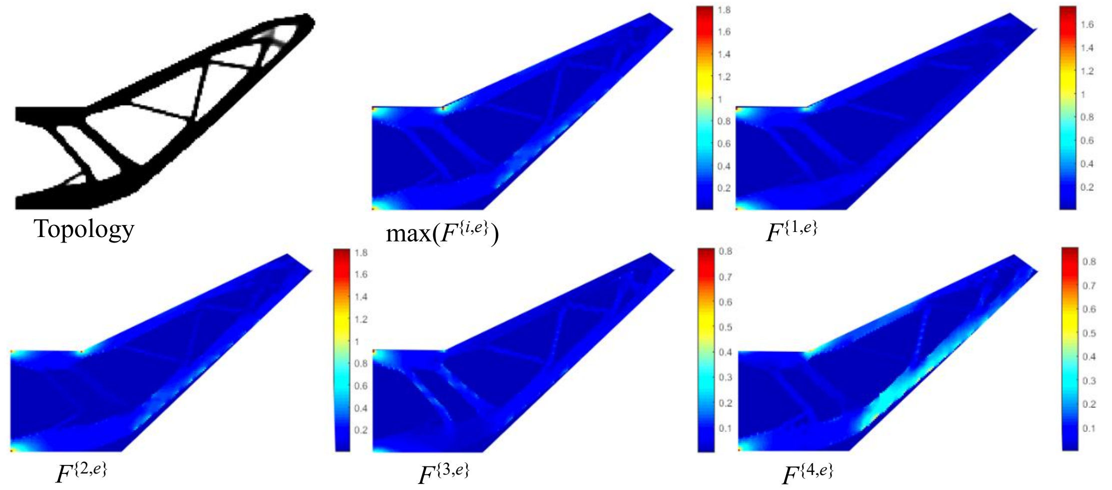

(a) Without stress control, v_F=0.5, C=441, max($F^{\{i,e\}}$)=1.826

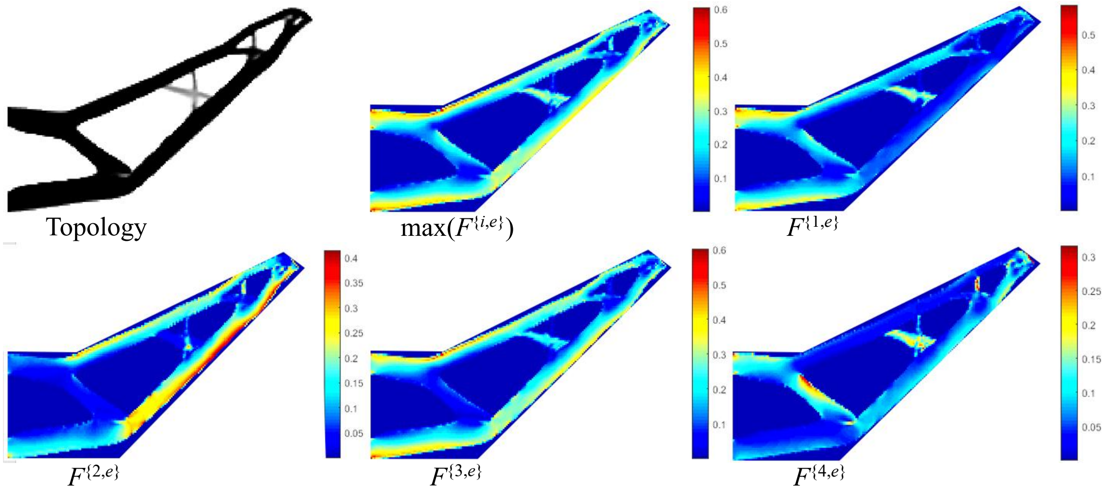

(b) With stress control, v_F=0.5, C=3291, max($F^{\{i,e\}}$)=0.604

Figure 36. The distribution of the Tsai-Hill failure indexes of the optimal antenna support bracket with a DD layup of [±68°/±22°]$_4$ using the proposed nested p-norm method.

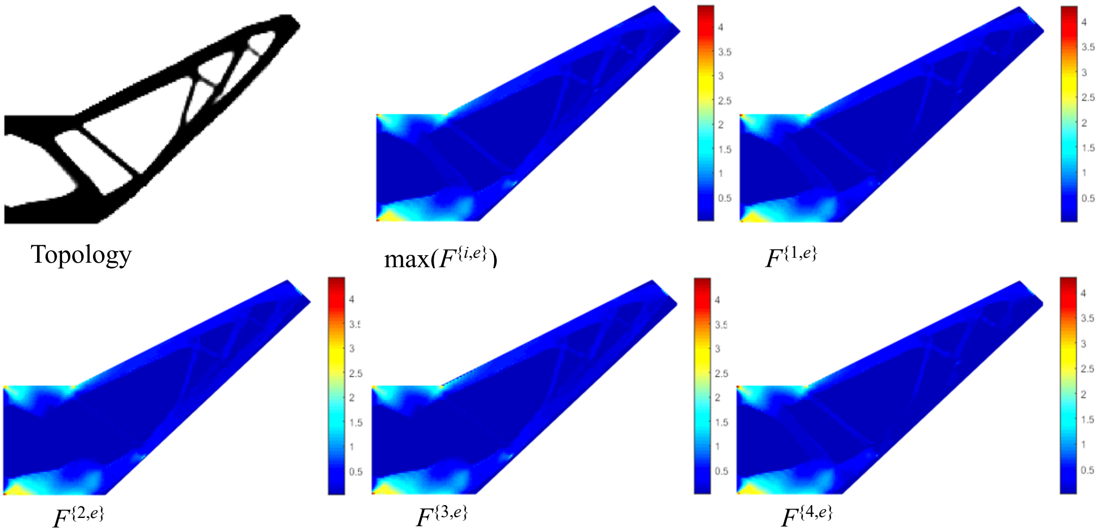

(a) Without stress control, v_F=0.5, C=4510, max($F^{\{i,e\}}$)=4.443

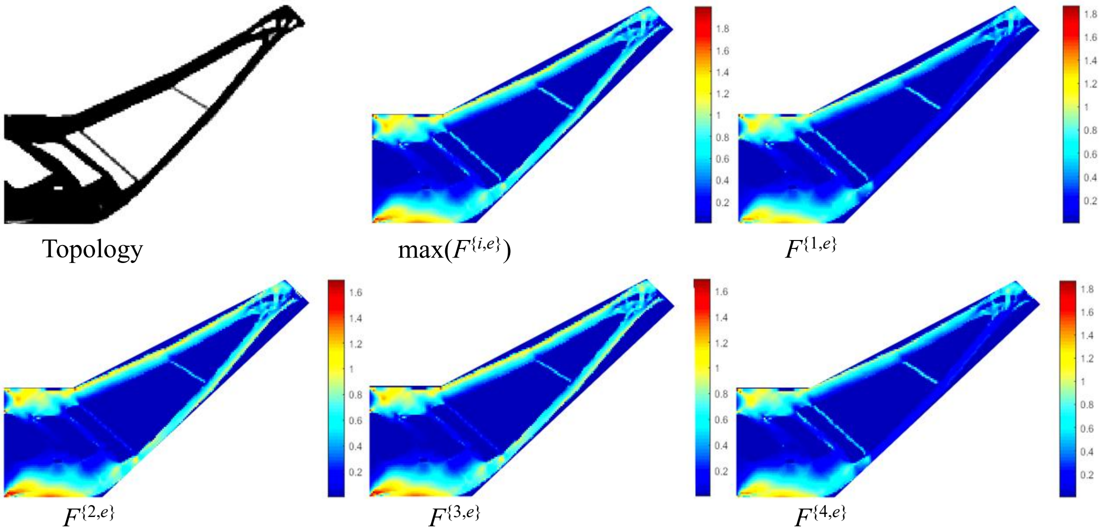

(b) With stress control, v_F=0.5, C=5321, max($F^{\{i,e\}}$)=1.999

Figure 37. The distribution of the Tsai-Hill failure indexes of the optimal antenna support bracket with a DD layup of [±45°]$_8$ using the proposed nested p-norm method.

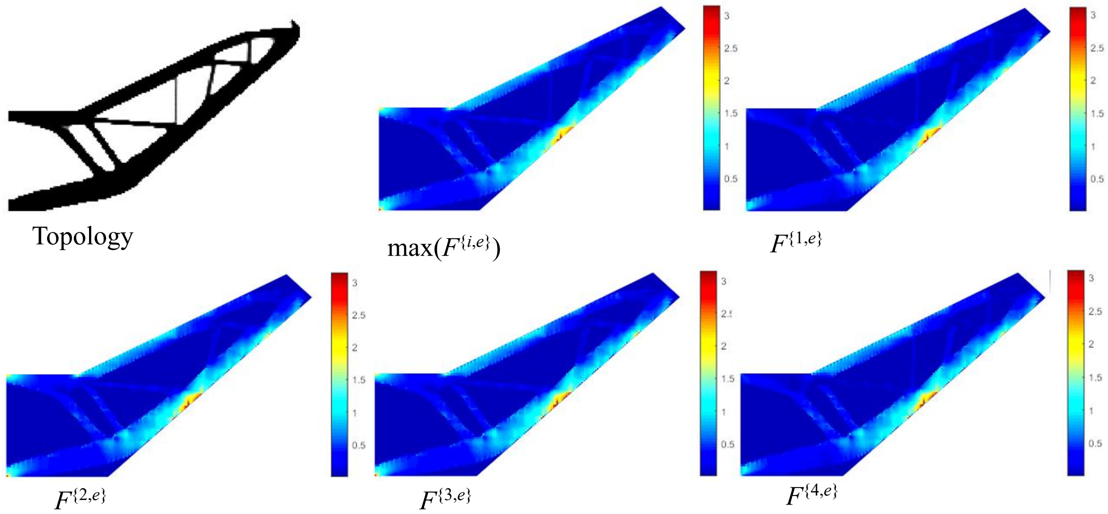

(a) Without stress control, v_F=0.5, C=4633, max($F^{\{i,e\}}$)=3.146

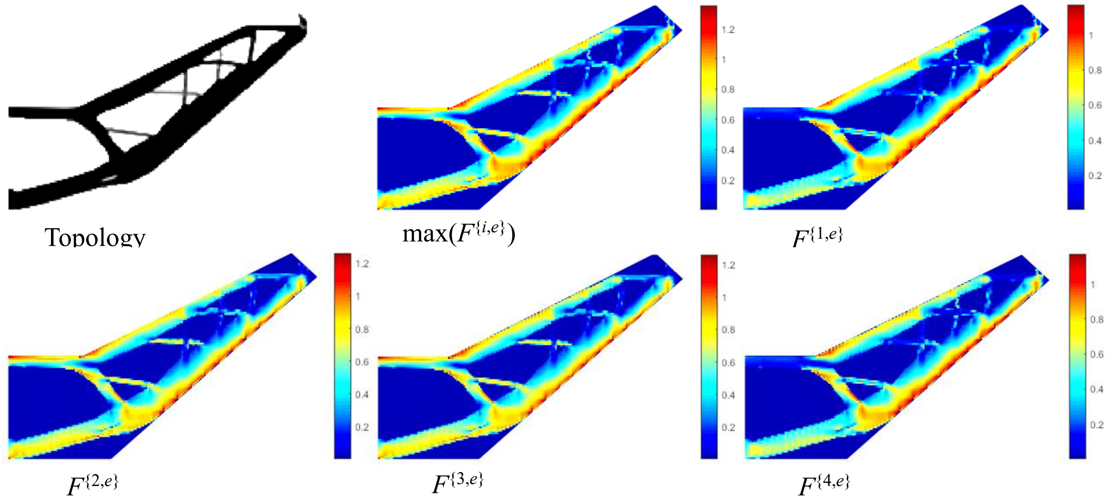

(b) With stress control, v_F=0.5, C=5069, max($F^{\{i,e\}}$)=1.352

Figure 38. The distribution of the Tsai-Hill failure indexes of the optimal antenna support bracket with a DD layup of [0°/90°]$_8$ using the proposed nested p-norm method.

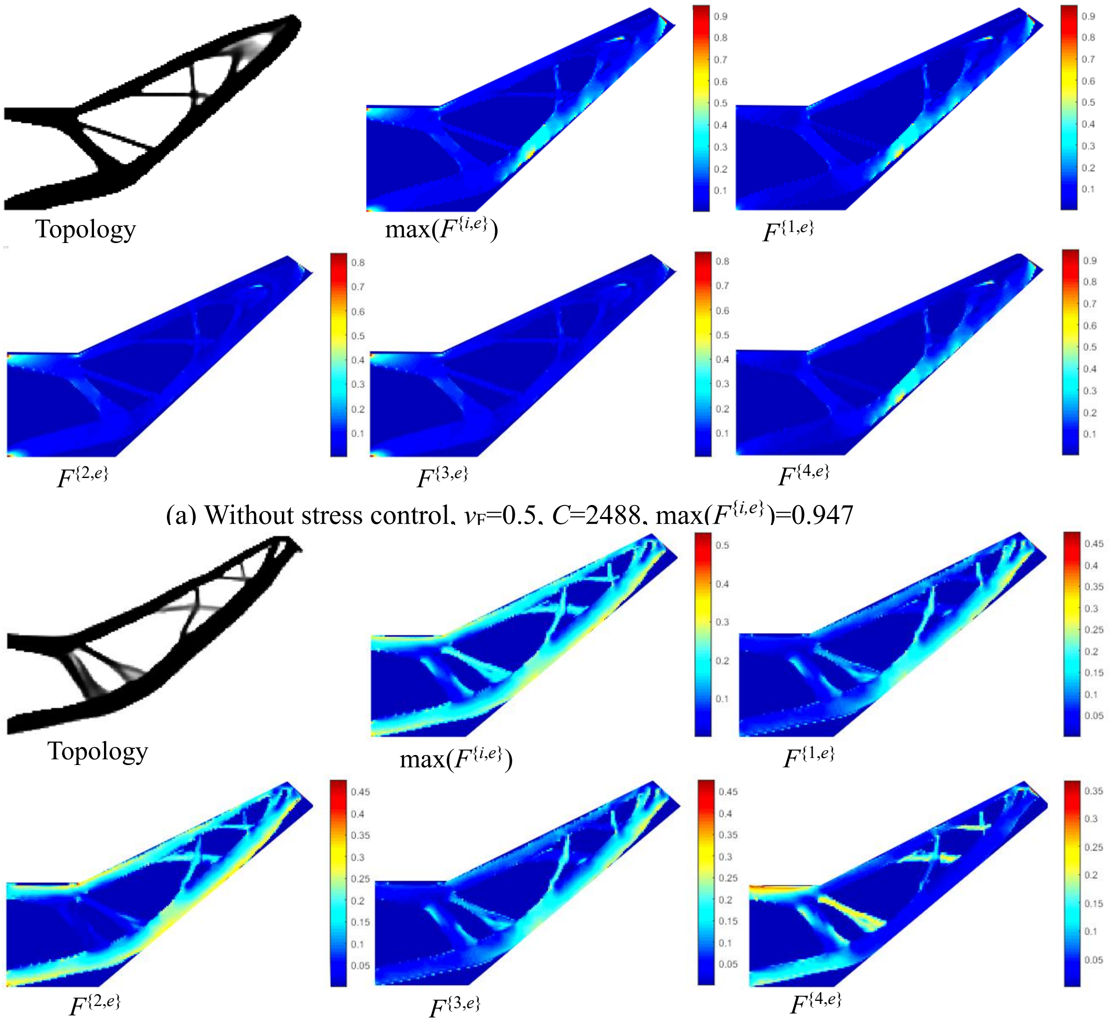

(b) With stress control, v_F=0.5, C=2854, max($F^{\{i,e\}}$)=0.532

Figure 39. The distribution of the Tsai-Hill failure indexes of the optimal antenna support bracket with a DD layup of $[\pm 0^{\circ}/\pm 50^{\circ}]_4$ using the proposed nested p-norm method.

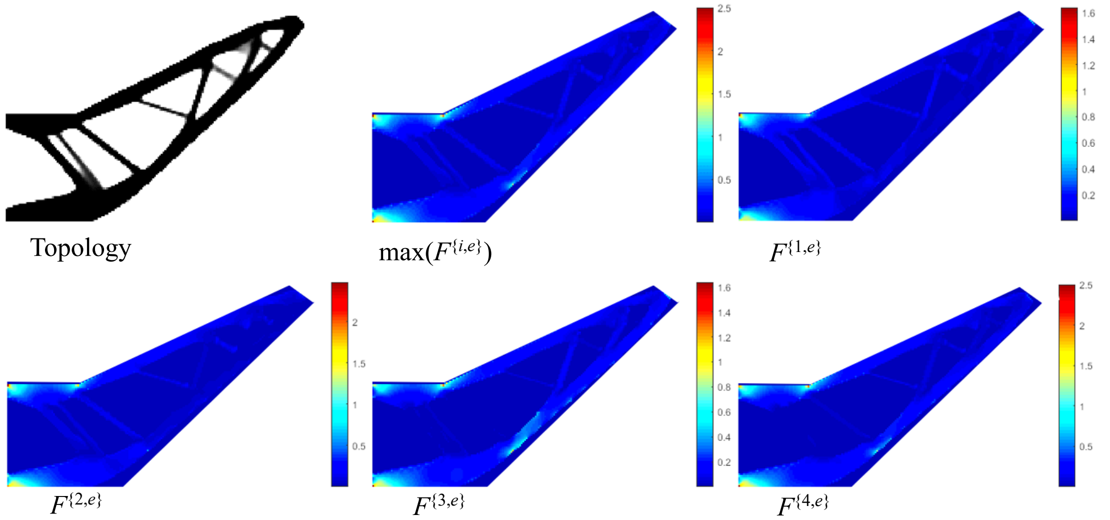

(a) Without stress control, v_F=0.5, C=3227, max($F^{\{i,e\}}$)=2.507

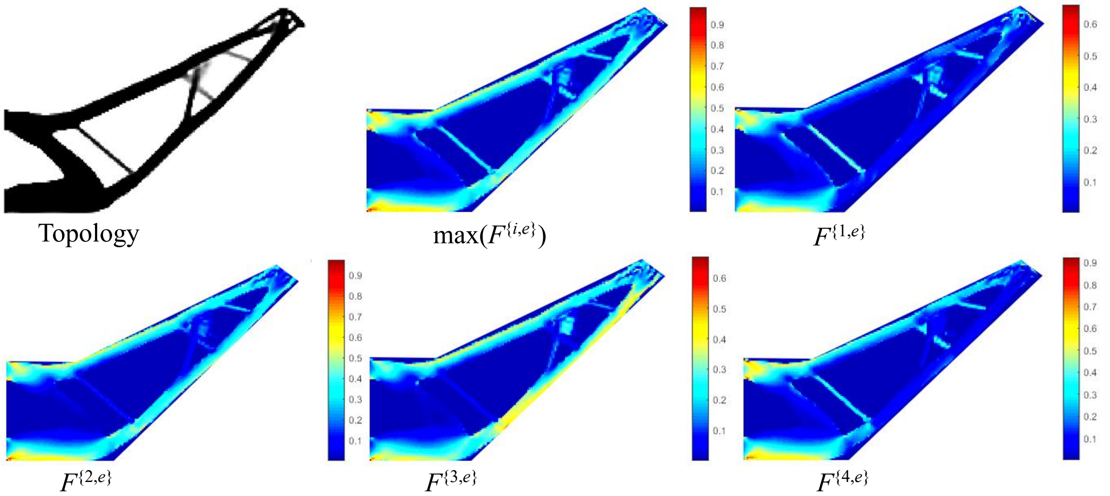

(b) With stress control, v_F=0.5, C=3730, max($F^{\{i,e\}}$)=0.979

Figure 40. The distribution of the Tsai-Hill failure indexes of the optimal antenna support bracket with a DD layup of [±32°/±58°]$_4$ using the proposed nested p-norm method.

5. Conclusions

In this paper, topology optimization of a novel double-double (DD) laminate is investigated considering stress control. To reduce the number of stress responses, a nested p-norm method is particularly proposed to integrate the Tsai-Hill failure indexes for different layers and different elements into one formulation. In the FE simulation, the SIMP model for isotropic material is extended to DD laminates for interpolating the material stiffness matrix of DD laminates with a penalty on the intermediate pseudo densities. After that, an optimization model is established to minimize the nested p-norm of the Tsai-Hill failure indexes with the constraint of the structural volume fraction. A large compliance constraint is added to guide the convergence of the optimization process. The computational efficiency is successfully improved by separately calculating the sensitivity of the filtered projection density using the adjoint method. Finally, typical numerical examples with stress concentrations including an L-shaped bracket, a crack problem, a corbel model and an antenna support bracket are used to validate the effectiveness and efficiency of the proposed nested p-norm method. The optimization results can give the following conclusions.

(1) It is shown that the proposed nested p-norm method can significantly reduce the stress concentration compared to the use of a minimum compliance optimization model without a

stress control, thereby turning a structure with a great risk of failure into a structure that will not fail. Meanwhile, the load bearing of the optimal structure considering the stress control is more uniform and reasonable.

(2) The proposed nested p-norm is proved to be the most effective and efficient method to solve the stress problem of composite laminates when compared with the methods using single p-norm and layer-wise p-norm. The different effects of elements and layers on stress constraints are not distinguished in the single p-norm method, which will lead to a large number of local optimal solutions, preventing the optimization process from converging to an effective solution. Using the layer-wise p-norm, the number of design constraints will be multiplied by the number of representative layers. The proposed nested p-norm has advantages in both effectiveness and computational efficiency.

(3) The optimized configurations obtained by DD laminates and Quad laminates with the equivalent QI stiffness are very similar. Optimization results of different DD laminates shows that the stress concentration in the optimal configurations is closely related to laminate layups. It is difficult for some layups to achieve the ideal stress distribution even through topology optimization for specific loaded structures, such as the laminate with the layup of $[0^{o}/90^{o}]_8$ for the L-shaped bracket, and soft laminates with the layups of $[\pm 45^{o}]_8$ and $[\pm 32^{o}/\pm 58^{o}]_4$ for the crack problem and the corbel structure. With the current optimization algorithm, suitability of layup design can be evaluated for certain loading cases.

(4) The last example for the optimized design of the antenna support bracket, although simplified, verifies the application potential of the proposed nested p-norm method in complex engineering structures.

Finally, it should be noted that the effectiveness of the proposed nested p-norm method for reducing the stress concentration in topology optimization of DD laminates is validated by comparing with the optimization problems for minimizing the compliance under the same volume fraction. The proposed method can also be used for other optimization problems with stress constraints, such as minimizing the volume by including the stress and the compliance constraints.

Acknowledgment

Zhong Yucheng acknowledges the financial support from National Natural Science Foundation of China (12202325).

Dan Wang acknowledges the financial support by A*STAR (C210812010, A19C9a0044).

References

[1] H. A. Eschenauer, N. Olhoff, Topology optimization of continuum structures: a review, Applied Mechanics Reviews, 54 (4) (2001) 331-390.
doi: 10.1115/1.1388075

[2] M. P. Bendsoe, O. Sigmund. Topology optimization: theory, methods, and applications. Springer Berlin, Heidelberg, 2002
doi: 10.1007/978-3-662-05086-6

[3] G.I.N. Rozvany, A critical review of established methods of structural topology optimization, Structural and Multidisciplinary Optimization, 37 (2009) 217-237.
doi: 10.1007/s00158-007-0217-0

[4] M.P. Bendsøe, Optimal shape design as a material distribution problem, Structural Optimization, 1 (1989) 193-202.
doi: 10.1007/BF01650949

[5] M.P. Bendsøe, O. Sigmund, Material interpolation schemes in topology optimization, Archive of Applied Mechanics, 69 (1999) 635-654.
doi: 10.1007/s004190050248

[6] X. Huang, Y. Xie, A further review of ESO type methods for topology optimization, Structural and Multidisciplinary Optimization, 41 (2010) 671-683.

doi: 10.1007/s00158-010-0487-9
[7] L. Xia, Q. Xia, X. Huang, Y. Xie, Bi-directional Evolutionary Structural Optimization on Advanced Structures and Materials: A Comprehensive Review, Archives of Computational Methods in Engineering. 25 (2018) 437-478. doi: 10.1007/s11831-016-9203-2
[8] D. Yang, H. Liu, W. Zhang, S. Li, Stress-constrained topology optimization based on maximum stress measures, Computers & Structures. 198 (2018) 23-39. doi: 10.1016/j.compstruc.2018.01.008
[9] B. Xu, Y. Han, L. Zhao, Bi-directional evolutionary topology optimization of geometrically nonlinear continuum structures with stress constraints, Applied Mathematical Modelling. 80 (2020) 771-791. doi: 10.1016/j.apm.2019.12.009
[10] G. Allaire, F. Jouve, A. Toader, A level-set method for shape optimization, Comptes Rendus Mathematique, 334(12) (2002) 1125-1130. doi: 10.1016/S1631-073X(02)02412-3
[11] G. Allaire, C. Dapogny, P. Frey, Shape optimization with a level set based mesh evolution method, Computer Methods in Applied Mechanics and Engineering, 282 (2014) 22-53. doi: 10.1016/j.cma.2014.08.028
[12] M. Y. Wang, X. Wang, D. Guo, A level set method for structural topology optimization, Computer Methods in Applied Mechanics and Engineering. 192 (1) (2003) 227-246. doi: 10.1016/S0045-7825(02)00559-5
[13] Q. Xia, M. Y. Wang, Topology optimization of thermoelastic structures using level set method, Computational Mechanics, 42 (2008) 837-857. doi: 10.1007/s00466-008-0287-x
[14] L. Xia, P. Breitkopf, Multiscale structural topology optimization with an approximate constitutive model for local material microstructure, Computer Methods in Applied Mechanics and Engineering, 286 (2015) 147-167. doi: 10.1016/j.cma.2014.12.018
[15] J. Gao, Z. Luo, L. Xia, L. Gao, Concurrent topology optimization of multiscale composite structures in Matlab, Structural and Multidisciplinary Optimization, 60 (2019) 2621-2651. doi: 10.1007/s00158-019-02323-6
[16] M. Xiao, D. Lu, P. Breitkopf, B. Raghavan, S. Dutta, W. Zhang, On-the-fly model reduction for large-scale structural topology optimization using principal components analysis, Structural and Multidisciplinary Optimization, 62 (2020) 209-230. doi: 10.1007/s00158-019-02485-3
[17] S. Mukherjee, D. Lu, B. Raghavan, P. Breitkopf, S. Dutta, M. Xiao, W. Zhang, Accelerating large-scale topology optimization: State-of-the-art and challenges, Archives of Computational Methods in Engineering, 28 (2021) 4549-4571. doi: 10.1007/s11831-021-09544-3
[18] H. Ghasemi, H.S. Park, T. Rabczuk, A level-set based IGA formulation for topology optimization of flexoelectric materials, Computer Methods in Applied Mechanics and Engineering, 313 (2017) 239-258. doi: 10.1016/j.cma.2016.09.029
[19] W. Zhang, D. Li, P. Kang, X. Guo, S.-K. Youn, Explicit topology optimization using IGA-based moving morphable void (MMV) approach, Computer Methods in Applied Mechanics and Engineering, 360 (2020) 112685. doi: 10.1016/j.cma.2019.112685
[20] L. Xia, J. Yvonnet, S. Ghabezloo, Phase field modeling of hydraulic fracturing with interfacial damage in highly heterogeneous fluid-saturated porous media, Engineering Fracture Mechanics. 186 (2017) 158-180. doi: 10.1016/j.engfracmech.2017.10.005
[21] W. Zhang, J. Yuan, J. Zhang, X. Guo, A new topology optimization approach based on Moving Morphable Components (MMC) and the ersatz material model, Structural and Multidisciplinary Optimization. 53 (201) 1243-1260. doi: 10.1007/s00158-015-1372-3

[22] W. Zhang, J. Chen, X. Zhu, J. Zhou, D. Xue, X. Lei, X. Guo, Explicit three dimensional topology optimization via Moving Morphable Void (MMV) approach, Computer Methods in Applied Mechanics and Engineering. 322 (2017) 590-614.
doi: 10.1016/j.cma.2017.05.002

[23] Y. Zhou, W. Zhang, J. Zhu, Z. Xu, Feature-driven topology optimization method with signed distance function, Computer Methods in Applied Mechanics and Engineering, 310 (2016) 1-32.
doi: 10.1016/j.cma.2016.06.027

[24] J. Sokolowski, A. Zochowski, On the Topological Derivative in Shape Optimization, SIAM Journal on Control and Optimization. 37 (4) (1999)1251-1272.
doi: 10.1137/S0363012997323230

[25] J.A. Norato, M. P. Bendsøe, R. B. Haber, D. A. Tortorelli, A topological derivative method for topology optimization, Structural and Multidisciplinary Optimization, 33 (2007) 375-386.
doi: 10.1007/s00158-007-0094-6

[26] M. Zhou, Y.K. Shyy, H.L. Thomas, Checkerboard and minimum member size control in topology optimization, Structural and Multidisciplinary Optimization. 21 (2001) 152-158.
doi: 10.1007/s001580050179

[27] F. Wang, B.S. Lazarov, O. Sigmund, On projection methods, convergence and robust formulations in topology optimization, Structural and Multidisciplinary Optimization. 43 (6) (2011) 767-784.
doi: 10.1007/s00158-010-0602-y

[28] S. Zhang, J.A. Norato, A.L. Gain, N. Lyu, A geometry projection method for the topology optimization of plate structures, Structural and Multidisciplinary Optimization. 54 (2016) 1173-1190.
doi: 10.1007/s00158-016-1466-6

[29] H.Y. Lee, M. Zhu, J.K. Guest, Topology optimization considering multi-axis machining constraints using projection methods, Computer Methods in Applied Mechanics and Engineering. 390 (2022) 114464.
doi: 10.1016/j.cma.2021.114464

[30] Y. Xu, J. Zhu, Z. Wu, Y. Gao, Y. Zhao, W. Zhang, A review on the design of laminated composite structures: constant and variable stiffness design and topology optimization, Advanced Composites and Hybrid Materials, 1 (2018) 460-477.
doi: 10.1007/s42114-018-0032-7

[31] L. Meng, W. Zhang, D. Quan, G. Shi, L. Tang, Y. Hou, P. Breitkopf, J. Zhu, T. Gao, From topology optimization design to additive manufacturing: Today's success and tomorrow's roadmap, Archives of Computational Methods in Engineering, 27 (2020) 805-830.
doi: 10.1007/s11831-019-09331-1

[32] Y. Wang, Z. Wang, Z. Xia, L.H. Poh, Structural design optimization using isogeometric analysis: a comprehensive review, Computer Modeling in Engineering & Sciences, 117(3) (2018) 455-507.
doi: 10.31614/cmes.2018.04603

[33] P. Duysinx, M.P. Bendsøe, Topology optimization of continuum structures with local stress constraints, International Journal for Numerical Methods in Engineering. 43 (8) (1998) 1453-1478.
doi: 10.1002/(SICI)1097-0207(19981230)43:8<1453::AID-NME480>3.0.CO;2-2

[34] G.D. Cheng, X. Guo, ε-relaxed approach in structural topology optimization, Structural Optimization. 13 (1997) 258-266.
doi: 10.1007/BF01197454

[35] M. Bruggi, On an alternative approach to stress constraints relaxation in topology optimization, Structural and Multidisciplinary Optimization. 36 (2008) 125-141.
doi: 10.1007/s00158-007-0203-6

[36] Youn Kyu Park. Extensions of Optimal Layout Design using the Homogenization Method, University of Michigan ProQuest Dissertations Publishing, 1995, 9527718.
https://hdl.handle.net/2027.42/129559

[37] E. Holmberg, B. Torstenfelt, A. Klarbring, Stress constrained topology optimization, Structural and Multidisciplinary Optimization. 48 (2013) 33-47.
doi: 10.1007/s00158-012-0880-7

[38] G. Kreisselmeier, R. Steinhauser, Systematic Control Design by Optimizing a Vector Performance Index, IFAC Proceedings Volumes, 12(7) (1979) 113-117. doi: 10.1016/S1474-6670(17)65584-8
[39] J. París, F. Navarrina, I. Colominas, M. Casteleiro, Topology optimization of continuum structures with local and global stress constraints, Structural and Multidisciplinary Optimization. 39 (2009) 419-437. doi: 10.1007/s00158-008-0336-2
[40] K. Lee, K. Ahn, J. Yoo, A novel P-norm correction method for lightweight topology optimization under maximum stress constraints, Computers & Structures, 171 (2016) 18-30. doi: 10.1016/j.compstruc.2016.04.005
[41] C.-J. Thore, E. Holmberg, A. Klarbring, A general framework for robust topology optimization under load-uncertainty including stress constraints, Computer Methods in Applied Mechanics and Engineering, 319 (2017) 1-18. doi: 10.1016/j.cma.2017.02.015
[42] F.V. Senhora, O. Giraldo-Londoño, I.F.M. Menezes, G.H. Paulino, Topology optimization with local stress constraints: a stress aggregation-free approach, Structural and Multidisciplinary Optimization. 62 (2020) 1639-1668. doi: 10.1007/s00158-020-02573-9
[43] O. Giraldo-Londoño, G.H. Paulino, PolyStress: a Matlab implementation for local stress-constrained topology optimization using the augmented Lagrangian method, Structural and Multidisciplinary Optimization. 63 (2021) 2065-2097. doi: 10.1007/s00158-020-02760-8
[44] C. Jiang, J. Mi, S. Laima, H. Li, A novel algebraic stress model with machine-learning-assisted parameterization, Energies, 13(1) (2020) 258. doi: 10.3390/en13010258
[45] K. Svanberg, The method of moving asymptotes-a new method for structural optimization, International Journal for Numerical Methods in Engineering. 24 (2) (1987) 359-373. doi: 10.1002/nme.1620240207
[46] K. Svanberg. The Method of Moving Asymptotes (MMA) with Some Extensions. In: Rozvany, G.I.N. (eds) Optimization of Large Structural Systems. NATO ASI Series, vol 231. Springer, Dordrecht. (1993). doi: 10.1007/978-94-010-9577-8_26
[47] K. Svanberg, A class of globally convergent optimization methods based on conservative convex separable approximations, SIAM Journal on Optimization, 12(2) (2002) 555-573. doi: 10.1137/S1052623499362822
[48] S. Cai, W. Zhang, J. Zhu, T. Gao, Stress constrained shape and topology optimization with fixed mesh: A B-spline finite cell method combined with level set function, Computer Methods in Applied Mechanics and Engineering, 278 (2014) 361-387. doi: 10.1016/j.cma.2014.06.007
[49] S. Cai, W. Zhang, Stress constrained topology optimization with free-form design domains, Computer Methods in Applied Mechanics and Engineering, 289 (2015) 267-290. doi: 10.1016/j.cma.2015.02.012
[50] S. Cai, W. Zhang, An adaptive bubble method for structural shape and topology optimization, Computer Methods in Applied Mechanics and Engineering, 360 (2020) 112778. doi: 10.1016/j.cma.2019.112778
[51] D. Yu, S. Cai, T. Gao, W. Zhang, A 168-line MATLAB code for topology optimization with the adaptive bubble method (ABM), Structural and Multidisciplinary Optimization, 66 (2023) 10. doi: 10.1007/s00158-022-03403-w
[52] Z. Xu, W. Zhang, T. Gao, J. Zhu, A B-spline multi-parameterization method for multi-material topology optimization of thermoelastic structures, Structural and Multidisciplinary Optimization, 61 (2020) 923-942. doi: 10.1007/s00158-019-02464-8
[53] J. Zheng, G. Zhang, C. Jiang, Stress-based topology optimization of thermoelastic structures considering self-support constraints, Computer Methods in Applied Mechanics and Engineering, 408 (2023) 115957. doi: 10.1016/j.cma.2023.115957

[54] Q. Xia, T. Shi, S. Liu, M.Y. Wang, Shape and topology optimization for tailoring stress in a local region to enhance performance of piezoresistive sensors, Computers & Structures, 114-115 (2013) 98-105.
doi: 10.1016/j.compstruc.2012.10.020

[55] V. Keshavarzzadeh, R.M. Kirby, A. Narayan, Stress-based topology optimization under uncertainty via simulation-based Gaussian process. Computer Methods in Applied Mechanics and Engineering. 365 (2020) 112992.
doi: 10.1016/j.cma.2020.112992

[56] M. Bruggi, P. Duysinx, Topology optimization for minimum weight with compliance and stress constraints, Structural and Multidisciplinary Optimization. 46 (2012) 369-384.
doi: 10.1007/s00158-012-0759-7

[57] Y. Li, P.F. Yuan, Y.M. Xie, Topology optimization of structures composed of more than two materials with different tensile and compressive properties, Composite Structures, 306 (2023) 116609.
doi: 10.1016/j.compstruct.2022.116609

[58] Y. Zhou, T. Nomura, K. Saitou, Multi-component topology and material orientation design of composite structures (MTO-C). Computer Methods in Applied Mechanics and Engineering. 342 (2018) 438-457.
doi: 10.1016/j.cma.2018.07.039

[59] D. Harvey, P. Hubert, Extensions of the coating approach for topology optimization of composite sandwich structures, Composite Structures. 252 (2020) 112682.
doi: 10.1016/j.compstruct.2020.112682

[60] J. Wong, A. Altassan, D.W. Rosen, Additive manufacturing of fiber-reinforced polymer composites: A technical review and status of design methodologies, Composites Part B: Engineering, 255 (2023) 110603.
doi: 10.1016/j.compositesb.2023.110603

[61] S.T. IJsselmuiden, M.M. Abdalla, Z. Gürdal, Implementation of strength-based failure criteria in the lamination parameter design space, AIAA Journal, 46(7) (2008) 1826-1834.
doi: 10.2514/1.35565

[62] A. Khani, S.T. IJsselmuiden, M.M. Abdalla, Z. Gürdal, Design of variable stiffness panels for maximum strength using lamination parameters, Composites Part B: Engineering, 42(3) (2011) 546-552.
doi: 10.1016/j.compositesb.2010.11.005

[63] D.M.J. Peeters, G. G. Lozano, M. M. Abdalla, Effect of steering limit constraints on the performance of variable stiffness laminates, Computers & Structures, 196 (2018) 94-111.
doi: 10.1016/j.compstruc.2017.11.002

[64] Z. Hong, D. Peeters, Y. Guo, Efficient strength optimization of variable stiffness laminates using lamination parameters with global failure index, Computers & Structures, 271 (2022) 106856.
doi: 10.1016/j.compstruc.2022.106856

[65] D. Wang, M.M. Abdalla, W. Zhang, Buckling optimization design of curved stiffeners for grid-stiffened composite structures, Composite Structures, 159 (2017) 656-666.
doi: 10.1016/j.compstruct.2016.10.013

[66] D. Wang, M. M. Abdalla, W. Zhang, Sensitivity analysis for optimization design of non-uniform curved grid-stiffened composite (NCGC) structures, Composite Structures, 193 (2018) 224-236.
doi: 10.1016/j.compstruct.2018.03.077

[67] D. Wang, M. M. Abdalla, Z. Wang, Z. Su, Streamline stiffener path optimization (SSPO) for embedded stiffener layout design of non-uniform curved grid-stiffened composite (NCGC) structures, Computer Methods in Applied Mechanics and Engineering, 344 (2019) 1021-1050.
doi: 10.1016/j.cma.2018.09.013

[68] D. Wang, S.-Y. Yeo, Z. Su, Z. Wang, M. M. Abdalla, Data-driven streamline stiffener path optimization (SSPO) for sparse stiffener layout design of non-uniform curved grid-stiffened composite (NCGC) structures, Computer Methods in Applied Mechanics and Engineering, 365 (2020) 113001.
doi: 10.1016/j.cma.2020.113001

[69] A.A. Groenwold, R. T. Haftka, Optimization with non-homogeneous failure criteria like Tsai–Wu for composite laminates, Structural and Multidisciplinary Optimization, 32 (2006) 183-190.
doi: 10.1007/s00158-006-0020-3

[70] C. Kassapoglou, Design and analysis of composite structures: with applications to aerospace structures, 2nd Edition. John Wiley & Sons, 2013.

[71] S.W. Tsai, Double-double: New family of composite laminates, AIAA Journal, 59 (11) (2021) 1-11.
doi: 10.2514/1.j060659

[72] B. Vermes, S.W. Tsai, T. Massard, G.S. Springer, T. Czigany, Design of laminates by a novel "double-double" layup, Thin-Walled Structures. 165 (2021) 107954.
doi: 10.1016/j.tws.2021.107954

[73] E. Kappel, Double-Double laminates for aerospace applications-Finding best laminates for given load sets, Composites Part C: Open Access. 8 (2022) 100244.
doi: 10.1016/j.jcomc.2022.100244

[74] B. Vermes, S. W. Tsai, A. Riccio, F. C. Di, S. Roy. Application of the Tsai's modulus and double-double concepts to the definition of a new affordable design approach for composite laminates. Composite Structures, 259 (2021), 113246.
doi: 10.1016/j.compstruct.2020.113246

Appendix

By using the SIMP model, the material distribution is tailored by forcing the elemental pseudo densities associated with a discretized mesh to achieve either zero or one. It is found that there is a chance that the optimal material layout represents a pattern of the alternating regions of solid and void elements arranged in a checkerboard manner, which is the so-called checkerboard phenomena, as illustrated in Figure A1. These structures are not practically feasible due to the weak connection at the alternating joints. To avoid the checkerboard patterns, density filtering technologies based on image processing were proposed by Zhou et al. [33] and have been widely used in the SIMP-based topology optimization design.

Figure A1. Checkerboard phenomenon in topology optimization using the SIMP model.

For the *e*th element, its filtering area $\Omega_e^{(r)}$ is to draw a circle with radius r_0 at the elemental center, as illustrated in Figure A2. Elements centered inside the circle will participate in the density filtering of the *e*th element. The filter density is defined as the weighted average of adjacent design variables, with the expression of:

$$\tilde{x}_e = \frac{\sum_{j=\Omega_e} w_j x_j}{\sum_{j=\Omega_e} w_j} = \sum_{j=1}^{\Omega_e} w_{ej} x_j \tag{A1}$$

where x_e and $\tilde{x}_e$ are the original and the filtered pseudo densities associated to the *e*th element, respectively. The weight factor w_j is defined as:

$$w_j = \frac{r_0 - r_j}{r_0} \tag{A2}$$

where r_j denotes the center distance between the *e*th element and its surrounding *j*th element. From the definition, elements that are closer to the investigated element have a greater influence on the density of that element. The filtering effect linearly decreases with element distance. Noticeably, pseudo densities of elements outside the filtering area have no contributions to the filtering.

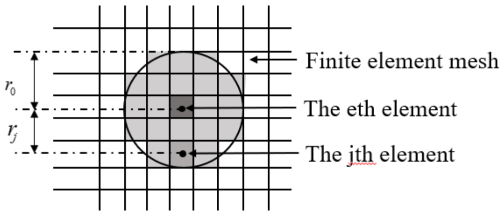

Figure A2. Illustration of the density filtering.

Density filtering can help to avoid checkerboard phenomena. However, there are still many gray elements and unclear imaging (no obvious boundary) for the optimal solutions. The projection method can help clarifying the boundaries. A concise expression using the tanh function is used here as the projection function [15]:

$$\rho_e = \frac{\tanh(\beta\eta) + \tanh(\beta(\tilde{x}_e - \eta))}{\tanh(\beta\eta) + \tanh(\beta(1-\eta))} \tag{A3}$$

where ρ_e is the projection density of the e^{th} element, η is the threshold to determine the material retention, and β is the degree of discreteness of the projection. Different η values correspond to the projection function as shown in Figure A3, and different β values correspond to different slopes. This alternative provides a faster way to calculate the projection, and when β approaches infinity, the same result as the original projection formula can be obtained. The condition η=0 guarantees the minimum size of the real phase (solid material), and η=1 guarantees the minimum size of the empty phase (removing the material part). Xu et al. and Kawamoto et al. indicate that convergence is smooth when η is close to 0.5 and for smaller values. The larger the value of β, the more discrete the result of the corresponding projection density.

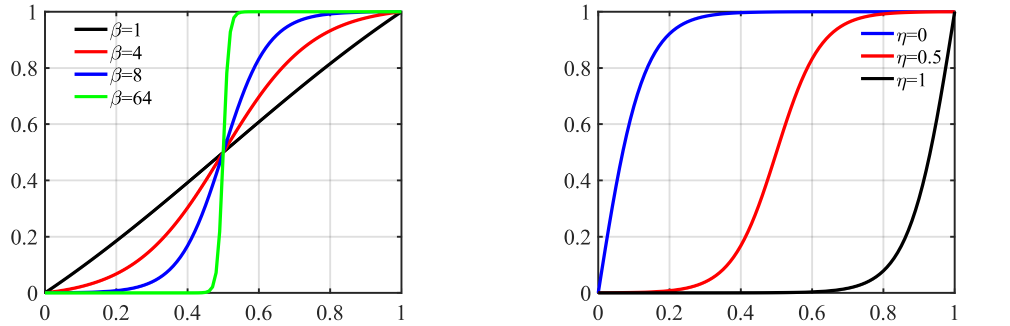

(a) A function of different β values at η=0.5 (b) A function of different η values at β=8

Figure A3. Projection density function.